SLAC PUB 6989
January 1996

Impedance Study for the PEP-II B-Factory*

S. HEIFETS, K. KO, C. NG, X. LIN, A. CHAO, G. STUPAKOV,
M. ZOLOTAREV, J. SEEMAN, U. WIENANDS,
C. PERKINS, M. NORDBY, E. DALY, N. KURITA, AND D. WRIGHT
Stanford Linear Accelerator Center, Stanford University, Stanford, CA 94309, USA

E. HENESTROZA, G. LAMBERTSON, J. CORLETT, J. BYRD, AND M. ZISMAN
Lawrence Berkeley Laboratory, Berkeley, CA 94720, USA

T. WEILAND
TechHochschule Darmstadt, Inst. fur Kernphysik, D-6100 Darmstadt, Germany

W. STOEFFL AND C. BOLSER
Lawrence Livermore National Laboratory, Livermore, CA 94350, USA

ABSTRACT

The paper summarizes results from the impedance study of the components of the PEP-II B-factory[1].

Presented at the International Workshop on Collective Effects and Impedance for B-Factories
Tsukuba, Japan, June 12 17, 1995

⋆ Work supported in part by Department of Energy contract DE–AC03–76SF00515.

Table 1. Parameters of the PEP-II B-factory

parameter		HER/LER	
energy	E	9.0/3.1	GeV
average radius	R	350.03	m
rf frequency	f_{rf}	476.0	MHz
harmonic number	h	3492	
revolution frequency	f_0	136.3	kHz
dc beam current	I_B	0.986/2.14	A
number of bunches	n_b	1658	
particles per bunch	N_B	$(2.72/5.91)\ 10^{10}$	
gap	$n_g; l_g$	88; $0.05{*}2\pi R$	
bunch spacing	s_B	1.26	m
momentum comp.	α	$(2.41/1.31)\ 10^{-3}$	
energy spread	δ	$(6.1/8.1)\ 10^{-4}$	
bunch length	σ_B	1	cm
damping time	τ_x	(36.8/40.4)	ms
z-Partition number	J_E	1.9969/2.0116	
number of cavities	n_{cav}	24/8	
loss/turn	U_0	3.57/0.87	MeV
synchrotron tune	Q_s	0.0516/0.033	
voltage/cavity	V_{rf}	0.77/0.64	MV
cavity shunt imped.	R_s	3.5	MΩ
average beta-x	β_x	(14.5/10.84)	m
average beta-y	β_y	(13.84/9.95)	m

Introduction

There is no need to emphasize how important it is to minimize the beam impedance for a lepton machine with the beam current of several amperes and a large number of bunches. This paper summarizes the results of the impedance studies of the components of the B factory[1]. The prime goal of this activity was to support the design of the vacuum chamber and, at the same time, to get a reasonable model of the machine impedance that can be used later for detailed studies of the collective effects. The work combined analytic approach and extensive simulations with available numerical codes such as MAFIA and ABCI.

The main parameters of the B factory relevant to the paper are given in Table 1.

In this paper we, first, discuss limitations on the impedance given by the beam dynamics. Next, we list the impedance-generating elements in the electron high-energy ring (HER) and mention the difference with the positron low-energy ring (LER). The analysis of the impedance of each element follows. At the end, we summarize results giving the parameters of the impedance of the HER.

Constraints on the impedance

Impedances should be minimized to reduce the wakefields excited by the beam, which may make the beam unstable. Coherent effects impose certain limitations on the magnitude of the impedance.

The longitudinal wakefield modifies the rf potential well and, as a result, changes the bunch shape $\rho(s)$. For a purely inductive impedance L, a single bunch self-consistent potential is

$$U = \frac{s^2}{2\sigma_B^2} + \Lambda L \rho(s) \tag{1}$$

where $\int \rho(s) ds = 1$, and dimensionless

$$\Lambda = \frac{N_B r_e}{2\pi\gamma\alpha\delta^2 R}, \quad r_e = \frac{e^2}{mc^2}, \quad \gamma = \frac{E}{mc^2}. \tag{2}$$

For small s,

$$U = [1 - \frac{\Lambda L}{\sigma_B \sqrt{2\pi}}] \frac{s^2}{2\sigma_B^2}. \tag{3}$$

For the HER at the nominal $I_B = 1\,A$, $\Lambda/\sqrt{2\pi} = 0.88510^{-3}$, and 10% bunch lengthening may be expected for

$$L = 225\ nH, \quad \text{or} \quad Z/n = 0.2\ \Omega. \tag{4}$$

Microwave longitudinal instability sets the limit on the effective impedance $(Z/n)_{eff}$, defined as Z/n averaged with the bunch spectrum

$$(\frac{Z}{n})_{eff} < \frac{2\pi\alpha(E/e)\delta^2}{I_{peak}}, \tag{5}$$

where, for a Gaussian bunch, the peak bunch current is $I_{peak} = I_{bunch}^{av}\sqrt{2\pi}R/\sigma_B$. For the nominal CDR[1], Table 1, the limit is $(\frac{Z}{n})_{eff} < 0.97$ Ohms for the HER and $(\frac{Z}{n})_{eff} < 0.14$ Ohms for the LER. Sometimes SPEAR scaling $(\frac{Z}{n})_{eff} = (\frac{Z}{n})(\sigma_B/b)^{1.68}$ is used to relate effective and machine impedances. For the average $< b >= 3.3$ cm machine impedance is 7.4 times larger than effective impedance, giving $(Z/n) = 7.2$ Ohms for the HER, and $(Z/n) = 1.03$ Ohms for the LER. However, SPEAR scaling may not necessarily be valid for PEP-II. Note that a purely inductive impedance does not lead to microwave instability.

Transverse microwave (transverse fast blow-up) instability limits effective broad-band impedance for a given average bunch current;

$$|Z_\perp| < \frac{4Q_s(E/e)b}{I_{bunch}^{av} < \beta_\perp > R}, \tag{6}$$

where Q_s is the synchrotron tune, and $< \beta >$ is the average transverse beta function. At nominal CDR currents, an average $< \beta_\perp >= 10$ m, and a beam aperture $b = 2.5$ cm, the criterion limits impedance to $|Z_\perp| = 21$ MΩ/m for the HER, and $|Z_\perp| = 2.3$ MΩ/m for the LER.

Transverse mode-coupling instability limits the imaginary part of effective transverse impedance

$$ImZ_{\perp} < \frac{4Q_s(E/e)b}{I_{bunch}^{av} < \beta_{\perp} > R}\frac{4\sqrt{\pi}}{3}\frac{\sigma_B}{b}. \tag{7}$$

and gives essentially the same constraints for PEP-II as fast blow-up instability.

Slow head-tail instability sets a loose limit on the chromaticity of the ring and is not important for this note.

Transverse impedance also causes closed-orbit distortion and changes the betatron tune; however, these effects are small. They may be enhanced by a factor $Q_L c/(\pi f_m s_B)$ proportional to the loaded Q_L factor of a higher-order mode (HOM) excited by a train of bunches if the frequency of a mode f_m of the narrow-band impedance is in resonance with the bunch spacing $f_m s_B/c = integer + 1/4$, or with the frequency of a coherent coupled-bunch mode of the train.

The maximum kick from a single mode to a bunch centroid with the offset r is

$$\theta = \frac{\Delta p_{\perp}}{p} = \frac{4\pi N_B r_e}{Z_0 \gamma}(\frac{2r}{s_B})\frac{R}{Q}Q_L, \qquad r_e = \frac{e^2}{mc^2}, \tag{8}$$

provided that the mode frequency is in resonance with the bunch spacing.

For example, one of the strongest rf cavity dipole HOM, with parameters f = 1674.2 MHz, $R/Q = 0.31\ k\Omega/m$, and loaded $Q_L = 2134$, gives the maximum transverse impedance $Z_{\perp} = (R/Q)Q_L = 0.66\ M\Omega/m$. Take $N_B = 6 \times 10^{10}$, offset r = 1 cm, $\gamma = E/mc^2 = 6 \times 10^3$, $r_e = e^2/mc^2 = 2.8 \times 10^{-13} cm$. Then $\theta = 1.0 \times 10^{-5}$ is much smaller than the divergence angle within a beam. The HOM of a cavity with length l is equivalent to a quad with the focusing length $F = l/\theta$. The betatron tune shift given by the mode is $\Delta Q_{\perp} = -\beta_{\perp}/(4\pi F)$ and, for l = 10 cm, $\beta_{\perp}$ = 11 m, $\Delta Q_{\perp} = 4. \times 10^{-4}$. Hence, under the resonance condition the maximum tune shift due to the strongest HOM of the 8 rf cavities $\Delta Q_{\perp} = 0.6 \times 10^{-3}$ in the LER is still much smaller than the beam-beam tune shift ($\xi = 0.03$).

More limitations derive from coupled bunch instabilities.

In the longitudinal case, the growth rate for n_b equally spaced bunches

$$\frac{1}{\tau_n} = \frac{I_B \alpha}{4\pi(E/e)Q_s} \sum_{p=-\infty}^{\infty} \omega_{pn} e^{-(\omega_{pn}\sigma_B)^2} Re Z_l(\omega_{pn})$$

where $\omega_{pn} = \omega_{rev}[pn_b + n + Q_s]$, should be compared to the damping time $\tau_l = 20$ ms. (This conservative approach ignores additional possible Landau damping and head-tail effect). That limits the impedance at any resonance frequency $f = \omega_{pn}/2\pi$. For the CDR parameters of the rings:

$$(\frac{f}{GHz})(\frac{ReZ}{k\Omega})e^{-(2\pi f \sigma_B/c)^2} < 19.5\ (HER); \quad < 4.1\ (LER). \tag{9}$$

Similarly, comparison of the growth rate of the transverse coupled-bunch instability

$$\frac{1}{\tau_{\perp,n}} = \frac{I_B f_{rev} \beta_\perp}{(E/e)} \sum_{p=-\infty}^{\infty} e^{-(\omega_{pn}\sigma_B)^2} Re Z_\perp(\omega_{pn}), \tag{10}$$

where $\omega_{pn} = \omega_{rev}[pn_b + n + Q_\perp]$, with damping time $\tau_\perp = 40$ ms, limits the transverse impedance at any resonance frequency f_{pn} to

$$\frac{ReZ_\perp}{K\Omega/m} e^{-(\omega\sigma_B/c)^2} < 119.8\ (HER); \qquad < 26.6\ (LER). \tag{11}$$

The longitudinal loss factor gives the energy loss of a beam and defines the power deposited in the beam pipe by an uncorrelated train of bunches

$$P = \Delta E f_0 = \frac{Z_0 I_B^2 \kappa_l s_B}{4\pi}, \tag{12}$$

where $Z_0 = 120\pi\ \Omega$ is the impedance of the vacuum. For a 1 A current and $s_B = 1.26$ m, a loss factor of $\kappa_l = 1$ V/pC corresponds to $P = 4.16$ kW of microwave power.

In summary, the main limitations to impedance come from bunch lengthening, power deposition, and multibunch stability. Single-bunch stability does not seem to be a strong limiting factor.

Table 2. Impedance generating elements, HER PEP-II B factory

RF Cavities	RF cavities	24
	RF cavities tapers	48
Arcs	Copper chamber(m)	1440
	Dipole screens	192
	BPM	198
	Arc bellows module	198
	Collimators	2
	Dipole offsets	384
	Quad pump slots	198
	Arc flex jonts	198
	Flange/gap rings	398
	Early x-ray mask	6
Straights	SS 304L pipe (m)	760
	BPM	92
	Collimators	6
	Pump ports	92
	Sliding joints	92
	Flex joints	92
	Flange/gap rings	184
	Gate valves	16
	Tapers octag./round	12

IR	IR Be chamber	1
	IR masks	
	Q2 septum	2
	Collimators	4
	IR pump ports	2
	Special BPMs	2
	High power dumps	2
Feedback	Feedback pickups	4
	Longitud. kicker	1
	Transverse kicker	1
Inject/Abort	Injection port	1
	Kicker ceramic	3
	Abort dump port	1
Arcs Diagnos.	Synch. light monitor	2
	SSRL xray port	2
Str. Diagnos.	BB curent monitors	1
	DC current transf.	1
	Tune monitor	1
	Profile monitor	1
IR Diagnos.	Luminosity monitor	1
Other	Pulsed separator	4
	PPS stopper	1

Impedances of the components

The list of impedance-generating elements in the HER (including interaction region (IR)) is given in Table 2. The LER is different in only a few aspects. First, the LER has an Al vacuum chamber in the arcs and, because LER dipoles are short, an ante-chamber with discrete pumps is used instead of HER distributed ion pumps (DIPs). In the LER, the impedance of the antechamber "replaces" the impedance of the dipole screens of the HER. Secondly, wigglers give an additional contribution to the LER impedance budget.

RF cavities

The dominant contribution to the impedance comes, of course, from the damped rf cavities (see Fig. 1).

The loaded Q_L factor of the HOMs for a damped cavity is relatively low and the width of a HOM is large compared to the revolution frequency. For this reason, the variation of the HOM frequency in the non-identical cavities (HOM detuning) is not important and the total impedance of the cavities is proportional to the number of cavities.

Table 3 summarizes the main longitudinal monopole and transverse dipole modes found numerically with the code URMEL and those measured on a prototype cavity[1].

The total narrow-band loss factor of a cavity is $\kappa_l = 0.26$ V/pC. This is the sum of the loss-factors of the monopole HOMs below the 2.5 GHz cut-off frequency of the beam pipe with $b = 4.76$ cm radius. The loss factor of the fundamental mode adds 0.167 V/pC. The total loss factor of a cavity calculated by ABCI from the wake field excited by a bunch going through the cavity is $k_l = 0.55$ V/pC; hence, the broad-band loss from the modes above the cut-off frequency is 0.12 V/pC.

The longitudinal wake-field of a rf cavity is depicted in Fig. 2 and for dipole HOMs in Fig. 3. The real part of rf cavity longitudinal broad-band impedances is depicted in Fig. 4. The beam-pipe radius is $b = 4.49$ cm.

Table 3. Single RF Cavity Monopole HOMs

	freq (MHz)	R/Q	$R_s(M\Omega)$	Q_L(num/mes)	$(R/Q)Q_L(k\Omega)$
1	489.6	108.8	5.036	/31926	3472.28
2	769.8	44.97	1.782	26/28	1.26
3	1015.4	0.006	0.0002	169/246	0.001
4	1291.0	7.68	0.692	66/	not visible
5	1295.6	6.57	0.265	/907	5.96
6	1585.5	5.06	0.216	/178	0.90
7	1711.6	4.75	0.404	not visible	
8	1821.9	0.06	0.006	/295	/0.018
9	1891.0	1.68	0.075	not visible	
10	2103.4	3.52	0.235	/233	0.82
11	2161.9	0.02	0.002	/201	0.004
12	2252.2	1.21	0.068	/500	0.61

Table 4. Main RF cavity Dipole HOMs, $r_0 = 4.7625$ cm

	f (MHz)	R/Q (Ω)	Q_L(calc/meas)	$(R/Q)(Q_L/kr_0^2\,(k\Omega/m)$
1	679.6	0.001	35/-	not visible
2	795.5	9.876	121/122	31.86
3	1064.8	31.990	38/-	not visible
4	1133.2	0.320	76/112	0.65
5	1208.2	0.385	2266/1588	10.3
6	1313.2	10.336	/498	80.1
7	1429.0	5.999	/3955	342.0
8	1541.0	2.065	/59	1.62
9	1586.2	5.262	/178	12.1
10	1674.2	14.732	/2134	385.0
11	1704.4	0.285	/444	1.52
12	1761.9	0.330	/7129	27.3

Eight cavities in the LER with the nominal beam current would generate 16.6 kW of power, see Eq. (12), propagating downstream from the cavities and absorbed in the walls. For TM modes in the round pipe with the radius $r = b$, the power absorbed in the wall within the distance $l = 1/\alpha_P$ is $P(z) \propto e^{-\alpha_P z}$, where

$$\alpha_P = \frac{k}{k_z}\frac{\delta}{b}.$$

Here, $k = \omega/c$, $k_z = \sqrt{k^2 - k_m^2}$, and k_m is the cut-off frequency of the m-th propagating mode. The bunch spectrum starts to roll off above frequencies $k\sigma \simeq 1$. For a $\sigma_B = 1$ cm bunch, the roll off starts at the frequency $f \simeq 4.77$ GHz. For such a frequency the skin depth is $\delta \simeq 1\mu m$ and the absorbtion length in the beam pipe with radius $b = 4.76$ cm is of the order of $l \simeq 500$ m. Hence, the wall power deposition from the cavities is $29.0\, W/m$. The broad-band transverse kick-factor of a rf cavity $k_\perp = 5.266$ V/pC/m at $b = 4.49$ cm.

The maximum narrow-band (NB) impedance of a single cavity $(R/Q)Q_L = 5.96\,\mathrm{k}\Omega$ at $f = 1.296$ GHz is larger than the $3.4\mathrm{k}\Omega$ limit set by Eq. (9) for the LER, see Table 3. The coherent stability of PEP-II therefore requires a feedback system. Optimization of the vacuum chamber should be considered, in this context, as an attempt to minimize requirements on the feedback system.

The same is true for the dipole modes. The dipole modes $f = 1.429$ GHz and $f = 1.674$ GHz have maximum impedances much higher than allowed by Eq. (11), see Table 4. Transverse stability depends again on the bunch-by-bunch transverse feedback system.

Resistive wall

The longitudinal resistive-wall impedance is given by[2]

$$\frac{Z_l}{n} = Z_0 \frac{(1-i)}{2}\frac{\delta}{b}\frac{L}{2\pi R} F(a/b). \tag{13}$$

where

$$\delta = \sqrt{\frac{2c}{Z_0 \sigma \omega}}$$

is the skin depth, $F = 1$ for a circular pipe with radius b, and $F(a/b) = 0.97$ for a rectangular beam pipe with a ratio of height-to-width of $b/a = 2.4/4.6 = 0.52$.

The transverse resistive-wall impedance for a circular pipe is

$$Z_\perp = \frac{2R}{b^2}\frac{Z_l}{n}. \tag{14}$$

The transverse impedance of a rectangular pipe can be estimated from the impedance of two parallel planes separated by a distance $2b$[3]:

$$Z_\perp = BZ_0 \frac{(1-i)}{2}\frac{2R}{b^2}\frac{\delta}{b}\frac{L}{2\pi R}. \tag{15}$$

$B = \pi^2/24$ or $B = \pi^2/12$ for motion parallel or perpendicular to the planes, respectively.

For the 1300 m copper beam pipe of the HER arcs with a conductivity $1/\sigma = 17.7$ n$\Omega - m$, the longitudinal and transverse impedances are $Z_l = 0.823(1-i)\sqrt{n}\Omega$, $Z_x = 0.435/\sqrt{n}$ MΩ/m, and $Z_y = 0.87/\sqrt{n}$ MΩ/m. The 900 m straight, circular stainless-steel pumps with $b = 4.6$ cm and $1/\sigma = 900$ n$\Omega - m$ give $Z_l = 2.16(1-i)\sqrt{n}$ Ω and $Z_\perp = 0.74/\sqrt{n}$ MΩ/m.

Combining the two contributions, the total resistive wall impedances are

$Z_l = 2.98(1-i)\sqrt{n}\ \Omega$, $Z_x = 1.175/\sqrt{n}$ MΩ/m, $Z_y = 1.61/\sqrt{n}$ MΩ/m.

The longitudinal impedance at the roll-off frequency of the bunch $k\sigma_B = 1$, or $n = 3.5 \times 10^4$, is 0.56 kΩ, still within the limit of Eq. (9). Transverse impedance gives the dominant contribution to the total impedance at low frequencies and is higher than the limit set by Eq. (11). Again, stability of the beam relies on a transverse feedback system.

The loss factor and the power deposition per unit length due to the resistive wall (RW) impedance in a circular beam pipe are

$$\frac{dk_l}{ds} = \frac{1}{2\pi b}\sqrt{\frac{2}{Z_0\sigma}}\frac{\Gamma(\frac{3}{4})}{\sigma_B^{3/2}}, \qquad \frac{dP}{ds} = \frac{e^2}{2\pi b}\frac{n_b N_B^2 f_0}{\sigma_B^{3/2}}\sqrt{\frac{2}{Z_0\sigma}}\Gamma(\frac{3}{4}), \tag{16}$$

where n_b is the number of bunches per ring, N_B is the number of particles per bunch, and f_0 is revolution frequency.

The copper coating on the stainless steel (SS) beam pipe may be used to reduce impedance and heating due to synchrotron radiation from upstream dipoles. The impedance depends on the thickness t of the coating: it decreases exponentially from the value for the SS pipe for $t = 0$ to the value of the copper pipe for $t \simeq \delta_{Cu}$ [4]

$$\frac{Z_l}{n} = Z_0\frac{(1-i)}{2}\frac{\delta}{b}\frac{L}{2\pi R}\zeta(t/\delta) \qquad (17),$$

where

$$\zeta(x) = \frac{1+\lambda+(1-\lambda)F(x)}{1+\lambda-(1-\lambda)F(x)}, \quad \lambda = \sqrt{\frac{\sigma_{SS}}{\sigma_{Cu}}}, \quad F(x) = e^{-2(1-i)x}. \tag{18}$$

The factor ζ goes to 1 for a thickness of the order of the skin depth of the coating.

The wall conductance at the transitions between arcs and straight sections has a jump. The impedance generated by such a jump in the conductivity may be estimated as the impedance of a step with a width equal to the difference of the skin depths and is negligible.

HER DIP screen

The screen separates the beam pipe and DIPs in the HER dipole vacuum chamber. We considered several possible screen designs. The issues here were the screen vacuum conductance, beam impedance, crosstalk between the plasma in the DIP and the beam, screening the beam from dust particles that may be produced in the DIP chamber, and screening the DIPs from scattered synchrotron radiation and from penetration of TE modes, which may be generated by an offset beam or by TM/TE mode conversion in the beam pipe. The impedance issue includes broad-band impedance as well as narrow-band impedance produced by the interference of waves generated by openings in the screen or by trapped modes.

The final screen design is based on T. Weiland's old idea of using continuous, narrow longitudinal grooves cut halfway through the screen with small holes cut through another half of the screen thickness (see Figs. 5a,b). Grooves with height w and depth d attenuate the beam field at the slot opening by a factor $e^{-\pi d/w}$ for frequencies $\omega/c < \pi/w$. For $w = 3$ mm, chosen for the grooves, this condition is true for all frequencies within the $\sigma_B = 1$ cm bunch spectrum. For $w = d$, the attenuation factor is $e^{-\pi} = 0.043$, and the broad-band impedance is reduced by the square of this factor, i.e. by a factor 500.

Narrow grooves also preclude the DIP plasma discharge affecting the beam. Continuous grooves reduce broad-band impedance and eliminate complications of narrow band impedance. Tilted grooves make efficient screening of the beam from dust particles and screening of the DIPs from scattered synchrotron radiation.

Small 3 mm diameter holes give large enough vacuum conductance while simultaneously preventing penetration of TE modes through the screen. A hole acts as an antenna for an incoming TE mode with a dipole moment proportional to r^3. The ratio of radiated power to incoming power of a TE wave generated in the beam pipe with radius b by a bunch with rms length σ_B may be estimated as (see Eq. A1-37)

$$\frac{\Delta U_{rad}}{\Delta U_{in}} \simeq 0.3(\frac{r^3}{b\sigma_B^2})^2. \tag{19}$$

Hence, the penetration length of a TE mode scales with the hole radius as $(1/r)^6$ and, for 3 mm holes, is larger then the absorbtion length of such modes in the beam-pipe walls. The hole separation is chosen large enough to make gap impedance small. This prevents a significant crosstalk between holes, which could result in the adding-up of their dipole moments. The mesh reduces total vacuum conductance by less than 4%. There will be 192 screens, 5.6 m long, with 6 grooves and 8400 holes per screen.

Each hole has an inductance $L = 3.5 \times 10^{-5}$ nH, giving $L = 56.5$ nH for all holes of the 192 screens. Attenuation in the grooves reduces the total inductance of the holes to $L = 0.1$ nH. The holes make the tolerance on the tilt of the grooves very loose in respect to the beam direction.

The total transverse impedance of the HER DIP screens is $Z_{\perp} = -i\,0.06\ k\Omega/m$.

The resistive part of the impedance and the loss factor for frequencies within the bunch spectrum are negligible small: $k_l = 5.5 \times 10^{-5}$ V/pC.

LER Antechamber

The LER antechamber replaces the DIP vacuum chamber of the HER and is similar to the antechamber of the ALS, see Figs. 6a,b. Impedance of the ALS antechamber was measured and modeled with MAFIA[5]. Broad-band impedance is generated mostly by the discontinuity of the antechamber slot at the ends. Narrow-band impedance would correspond to modes trapped in the antechamber. Simulations and theory show that the dependence of the impedance on the length of the slot saturates when it becomes several times the rms bunch length at several σ_B (several cm). Excitation of the modes of the antechamber by the beam may be attenuated significantly if the slot of the ante-chamber is narrow and long: it works exactly in the same way as to the grooves in the DIP screen. Fig. 7 shows the field pattern at the slot opening that confirms this statement. The attenuation factor found with MAFIA agrees with the simple formula $e^{-\pi d/w}$. However, the opening of the slot has to be large to accommodate the vertical size and the position jitter of the beam. Calculations were carried out with slot heights of 1.8, 1.4, and 1.0 cm. In all cases, the wake field is inductive and small, with maximum values of 0.04, 0.12, and 0.31 mV/pC, respectively, for a slot 40 cm long and 1 cm deep (see Fig. 8). Dependence on the depth c of the antechamber slot was compared for c = 1, 12, and 26 cm: the difference is negligible. The calculated inductive $Z/n = 0.5\ \mu\Omega$ or $L = 5.7 \times 10^{-4}$ nH is quite small and agrees with measurements. No trapped modes were found.

Abort system

The beam abort system requires a long vacuum chamber 3 cm wide and 12 cm deep (from the beam to the bottom) under the beam terminated with the dump[6] as shown in Figs. 9a, 9b. To minimize the impedance the chamber is screened with two shallow rf tapers (down and back up to the beam pipe). The taper going down may be very long and gives negligible impedance. The aborted beam goes through the taper going up. The angle α of this taper is limited by the energy deposition, which depends on radiation length X_0, and thickness t of the screen: $\alpha > t/X_0$. MAFIA calculations for a 3 m long structure with two (up and down) tapers 8.5 cm high and angle $\alpha = 0.048$, give an inductive wake field with $L = 0.23$ nH. The loss factor is $k_l = 4.5 \times 10^{-3}$ V/pC. No narrow-band trapped modes were found.

Interaction Region

The interaction region (IR) is a complicated 3-D set of masks and tapers as shown in Fig. 10a, and 10b. It was modeled as a whole structure using MAFIA. The broad-band wakefield is approximately inductive with $L = 5$ nH (see Fig. 11). The loss factor of the total structure is $k_l = 0.12$ V/pC. Most of the power lost due to the broad-band impedance propagates downstream and is absorbed outside the IR.

The main issue for the IR is heating. Heating in the IR results mostly from modes trapped in the central Be pipe ± 20 cm around the IP, 3 Watts of ohmic losses in the Be pipe, and, to a much smaller extent, from losses in upstream components of the beam pipe, mainly from the IR septum. Broad-band impedance has maximum $ReZ = 0.46\,\text{k}\Omega$ at 6 GHz as a result of averaging of the trapped modes.

The $l = 40$ cm Be pipe with radius $b = 2.5$ cm and adjacent masks with circular openings on both sides was modeled separately. The loss factor of this section is $k_l = 0.012$ V/pC. A number of the trapped modes are confined in the 40 cm Be pipe, due to the adjacent masks (see Fig. 12). Frequencies of the modes range from 4.6 GHz to 5.92 GHz. The frequency interval at the low-frequency end is about 50 MHz. Spacing increases to 150 MHz at the upper frequency end. Trapped modes are, basically, TM_{01} modes of the pill-box cavity with frequencies

$$\frac{\omega}{c} = \sqrt{(\frac{\nu}{b})^2 + (\frac{n\pi}{l})^2}. \tag{20}$$

The lowest radial number $\nu = 2.4$ and the number of the half waves n along the structure range from $n = 1$ to $n = 12$.

Both beams excite the modes simultaneously. For a symmetric structure, the amplitude A of the even modes ($n = 2m$) excited by a bunch is proportional to $(N_+ + N_-)\sin(kl/2)$, and for odd modes ($n = 2m + 1$), $A \propto (N_+ - N_-)\cos(kl/2)$ where $N_\pm$ is the number of particles per bunch in each beam. Therefore, the power deposited in even modes scales as $P \propto (N_+ + N_-)^2$. For an IP placed asymmetrically at a distance l_1 from one end of the pipe, the amplitude of the even and odd modes is

$$A_\pm \propto (N_+ + N_-)[\sin(kl_1) \pm \sin(kl_2)] + (N_+ - N_-)[\cos(kl_1) \mp \cos(kl_2)], \tag{21}$$

and odd modes can be excited even for equal number of particles in both beams. The power deposition within the Be pipe depends on the Q factor of the modes.

Resistive $Q \simeq 1.25\, 10^4$ is very large in our case. Loaded Q_L depends on the coupling of trapped modes to propagating modes in the beam pipe on the other side of the masks, where the beam pipe radius is much larger than that for the Be pipe. We estimate for round openings in the masks that

$$Q_{ext} \simeq (\frac{\pi f_m l}{c})(\frac{b}{a_0})^2 \frac{1}{W_t}, \tag{22}$$

where a_0 is the radius at the neck of the masks, and W_t is the probability of tunneling through the mask for a mode with frequency f_m:

$$W_t = |e^{-\int dz|q(z)|}|^2, \qquad |q(z)| = \sqrt{(\frac{\nu}{a(z)})^2 - (\frac{2\pi f_m}{c})^2}. \tag{23}$$

The integral may be estimated as

$$\int dz|q(z)| \simeq \frac{2\sqrt{2}}{3}\Delta^{3/2}\frac{\nu}{a'} \qquad \Delta = \frac{\nu c}{\omega_m a_0} - 1, \tag{23}$$

where $a' = |da/dz|$ is the slope of the mask.

For our case, this approach gives $Q_{ext} = 1200$ for a typical $f_m = 5.7$ GHz, and $a_0 = 1.5$ cm. In this case, only 10% of power loss goes to the Be pipe wall.

In principal, detuning from a resonance can be done by heating Be pipe. Temperature dependence of the mode frequency

$$\frac{\Delta f}{f} \simeq \frac{(\Delta l/l)}{1 + (\frac{\nu l}{\pi n b})^2} \tag{25}$$

is different for different n: the coefficient is equal to $1/50$ for $n = 1$, and $1/2$ for $n = 12$. For $(\Delta l/l) \simeq 10^{-5}\Delta T$, and $\Delta T \simeq 100^o$ the frequency shift for the mode $n = 12$ is small but comparable to the width of the resonance.

The power loss to an even mode with the loss factor κ_m and loaded Q_m^L is

$$P = P_0 D, \qquad P_0 = I_\Sigma^2 \kappa_m \frac{s_B}{c}, \tag{26}$$

where $P_0 = 480\,\mathrm{W}$ is the power loss of uncorrelated bunches, and $I_\Sigma = I_+ + I_-$. The enhancement factor D for a train of bunches with bunch spacing s_B

$$D = (\frac{c}{\omega_m s_B})\frac{1/Q_m^L}{(\Delta\omega_m/\omega_m)^2 + (1/2Q_m^L)^2} \tag{27}$$

depends on detuning the mode frequency from the resonance frequency ω_r, $\omega_r s_B/(2\pi c) =$ *integer*. Far away from the resonance $\Delta\omega_m/\omega_m >> 1/2Q_m$ and we get the factor $D << 1$. At the resonance

$$D_{max} = \frac{4Q_m^L c}{\omega_m s_B}, \tag{28}$$

and, for $s_B = 120$ cm and $f_m \simeq 6$ GHz, $D_{max} >> 1$ provided that $Q >> 70$. For $Q_m = 1200$, the enhancement $D_{max} = 16$, and $D_{min} = 4.4 \times 10^{-3}$. If only three out of twelve trapped modes are resonant, power loss is $P = 3 \times (1/12) \times 480W \times D_{max} = 1.92$ kW. Power dissipated into the wall itself is $P_{wall} = 192$ W in this case.

The frequency spectrum of a train of bunches also has frequencies at multiples of the revolution frequency ω_0. The number of independent coherent modes is equal to the number of bunches n_B. If the amplitude of the coherent mode is A_l, the power loss of a particle due to this mode is (Eq. A3-17)

$$P \simeq 2I_{av}^2(\frac{A_l\omega_l}{2c})^2(R/Q)_l Q_L^l. \tag{29}$$

The rms amplitude of the coherent modes is on the order of $A_l \simeq 2\sigma_B/\sqrt{n_B}$, and power loss due to single coherent mode is $2I_{av}^2(\sigma_B\omega_l/c)^2(Q_L/n_B)(R/Q)_l$. The number of such modes within the resonance width $\omega_l/(Q_L)$ is $\omega_l/(2Q_L\omega_0)$. Total loss of coherent modes

$$(2/\pi)(\sigma_B\omega_l/c)^2 P_0$$

is independent of Q_L and is smaller than the uncorrelated power loss P_0.

Hence, the wall-power loss is acceptable provided the pipe and adjacent masks are carefully designed to avoid resonances with bunch spacing.

Injection port, kicker ceramic

The injection port generates impedance due to a 2×12 cm slot in the tapered beam-pipe wall, with the average pipe radius $b = 3.8$ cm (see Fig. 13 a,b). Broad-band impedances, both of the slot and the taper, calculated with MAFIA, are mostly inductive. The slot gives an inductance $L = 0.025$ nH and a loss factor $k_l = 1.5 \times 10^{-3}$ V/pC. The contribution of the taper is larger: $L = 0.15$ nH and $k_l = 5.4 \times 10^{-3}$. Including both contributions, the injection port gives $L = 0.17$ nH and $k_l = 6.9 \times 10^{-3}$ V/pC. No indication of trapped modes was found.

Kicker ceramic section ($\epsilon = 9 >> 1$, thickness $\Delta b = 4$ mm, tube radius $b = 2.75$ cm) for the injection kicker (length $l = 1.25$ m) have a thin titanium coating (resistivity $\rho_{coat} = 43\ \mu\Omega - \text{cm}$). The wakefield generated by the ceramic section depends[7] on the parameter

$$V = \frac{\sigma_B \rho_{coat}}{Z_0(\Delta b)t}, \tag{30}$$

where $t = 0.75\mu m$ is the thickness of the coating. For this coating thickness, $V << 1$ and the wake

$$W(s) = \frac{2l}{tb}\frac{\rho_{coat}}{Z_0}\rho(s) \tag{31}$$

is mostly resistive, Eq. Appendix 1-22,

$$R_\Omega = \frac{l\rho_{coat}}{2\pi bt}. \tag{32}$$

For $l = 1.25$ m, the resistive part of the impedance $R_\Omega = 5.7\ \Omega$; the loss factor $k_l = 0.04$ V/pC. The inductive impedance corresponds to $L = 0.5\ 10^{-3}$ nH.

BPM

The HER has 290 sets of four-button BPMs (see Fig. 14). A BPM should have high sensitivity within the bandwidth 1 GHz, but at the same time must have low power going to the cables, low beam impedance, and low heating inside the BPM structure. We compared several designs of a BPM.

A 2 cm diameter round button is reasonably sensitive but the impedance is resonant at 6 GHz with relatively high shunt impedance. The problem may be avoided by making the button asymmetric. In particular, a narrow bridge across the gap eliminates the resonance but makes power to the cable too high. Measurements confirmed the results of MAFIA simulations quite well (see Figs. 15a,b).

The final version of the BPM uses a round button with $a = 1.5$ cm diameter. Such a design (see Fig. 16) satisfies requirements for sensitivity, heating, and power output to the cables.

For a four-button BPM and $N_B = 3 \times 10^{10}$, the sensitivity[9] is defined by the impedance 0.5Ω at 1 GHz.

The impedance of a single button is generated by a $w = 2$ mm round slot. Impedance of a slot can be estimated as the difference of the impedances of two round holes with radii a and $a + w$, giving polarizability $\alpha_e + \alpha_m = 2wa^2$ and

$$L = \frac{2wa^2}{\pi b^2},$$

or $L = 5.7 \times 10^{-3}$ nH per button, $L = 6.8$ nH for 300 four-button BPMs. The Kurennoy[8] estimate is smaller: $\alpha_e + \alpha_m = wa^2/8$. MAFIA[9] gives $L = 3.7 \times 10^{-2}11$ nH and a loss factor of $k_l = 2.7 \times 10^{-3}$ V/pC for a four-button BPM; $L = 11$ nH, and $k_l = 1$ V/pC for 300 BPMs.

Hence, the power loss by the beam is $P = 126$ W per BPM at the current 3A. Power output to a cable is found by direct calculations of the fields at the port and is 9 W per cable. The 1 cm beam offset in the direction to a button can increase power to the cable by a factor of 2 because the frequency harmonic of the field depends on the distance as $1/r$.

Transverse broad-band impedance of 300 BPMs found in simulations[9] is $Z_x = 6.7\,k\Omega/m$, and $Z_y = 5.5\,k\Omega/m$. One mode of the narrow-band longitudinal impedance has a total shunt impedance 6.5 $k\Omega$ at $f = 6.8$ GHz for 300 BPMs. The field pattern of the mode indicates that this mode is a TE_{11} mode (in respect to the button axis). Transverse narrow-band impedance Z_x has a mode with the total $R_s = 90\,k\Omega/m$ at $f = 6.8$ GHz, and $Z_y = 120\,k\Omega/m$ at $f = 6.2$ GHz.

The impedance is only slightly more than required by the conservative estimate of Eq. (9) and may increase the power of the feedback amplifier by not more than 5%.

Ceramic in the BPM has $\epsilon = 10$ and loss tangent of the ceramic is $\delta_c = 0.0007$. The power deposited by a propagating wave into ceramic with thickness $h = 3$ mm,

$$\frac{P}{P_{in}} = (\frac{\omega}{c})\frac{h}{2}\epsilon\delta_c, \tag{33}$$

is $P = 12$ mW per button for the loss $P_{in} = 126$ W per BPM at $f = 7.5$ GHz.

The power absorbed in the thin Ni layer at the edge of the ceramic in a coax with characteristic impedance $Z_W = (Z_0/2\pi)\ln(b/a)$ and radii a, b is

$$\frac{P}{P_{in}} = (\frac{\omega}{c})\frac{\mu\delta h}{d_{eff}}, \tag{34}$$

where for TEM wave

$$1/d_{eff} = \frac{(a+b)}{2ab\ln(b/a)}, \tag{35}$$

and δ is the skin depth of Ni. Note that $\mu\delta$ scales as $\sqrt{\mu}$. The permeability μ of Ni rolls off at high frequencies very rapidly and at 7 GHz is of the order $\mu = 3$ (see Fig. 17) reducing power loss to Ni to $P = 46.8mW$ per button for the loss $P_{in} = 126$ W per BPM.

The fraction of power absorbed in the resistive walls is on the order of the ratio of the length of a button $l = 1.9$ cm to the absorption length

$$\frac{P}{P_{in}} = (\frac{\omega}{c})\frac{\delta l}{d_{eff}} \tag{36}$$

and is very small.

The Q factor given by these losses is $Q_0 = 534$. The loaded Q_L, determined by MAFIA and confirmed in wire measurements on a BPM prototype, is much smaller: $Q_L \simeq 60$. It is too low to enhance the power loss in a train of bunches.

It is worthwhile to compare the loss factor $k_l = (\omega/2)(R/Q_0)$ of the longitudinal mode $f = 6.8$ GHz with the broad-band loss $k_l = 2.7 \times 10^{-3}$. Taking $Q_0 = Q_L$ and $R_s = 22\,\Omega$ per BPM, we get $k_l = 0.46/Q_L$ per BPM. This figure is larger than the broad-band loss factor for $Q_L = 100$. This argument indicates again that the loaded Q_L should be much less than Q_0 and has to be dominated by the radiation back to the beam pipe.

The relevant parameter for heating is the wall loss factor of a propagating wave multiplied by the number of passes of a wave, $Q_L c/\omega l \simeq 36$ for $Q_L = 60$. That gives absorbed power 2.5 W and heating of button at normal conditions should not be a problem.

If a button cable is accidentally disconnected, the situation may be different. First, reflection from the open unmatched end can produce a standing mode within the BPM. Consider a button as a transmission line. The currents and voltages at both ends of the line are related by the characteristic impedance of the line Z_L and the impedance of a termination Z_t:

$$V_{in} = V_t[\cos\psi + i\frac{Z_L}{Z_t}\sin\psi], \quad I_{in} = I_t[\cos\psi + i\frac{Z_t}{Z_L}\sin\psi].$$

Under normal conditions, the characteristic impedance of the line is matched to the impedance of the cable, and the voltage and current at both ends of the button are the same, except for a phase $\psi = ql$ where q is the propagating constant and l is the length of the line. For a disconnected cable, the current at the output port of the button is zero. The current at the input port is related to the density of the image current induced by the beam and, therefore, is the same as at the normal operation. Hence, voltage at the input port increases by a factor $\cot\psi$ compared to the normal operation. For a TEM wave with frequency ω, the phase ψ is $\psi = \omega l/c$. From a reciprocity theorem it follows that the voltage induced at the beam current and, hence, the energy loss by the beam and heating are also increased by the same factor $\cot\psi$, or by a factor 6.25 for $f = 7.5$ GHz and $l = 1.9$ cm. Radiation to the beam pipe is also increased due to the reflected TEM mode. Simulations with MAFIA confirmed appearance of the new resonances in the beam impedance with a disconnected cable.

The same design of BPMs with flat buttons will be used in the arcs and straight sections. In the straight sections, a flat button will be flush with the round beam pipe only at the center, making small cavities at the edges. The effect was simulated with MAFIA and changes the broad band impedance only by a few percents.

To screen BPMs from halo electrons, buttons will be recessed by 0.5 mm (including tolerance for installation). Other factors such as direct or secondary synchrotron radiation, or electrons emitted from the chamber walls are not affected by the small recess under consideration. For a beam pipe gap $b = 2.5$ cm and a betatron wave-length $\lambda_\beta \simeq 50$ m the incident angle of a halo electron is $\theta = 4b/\lambda_\beta$, and the recess $\Delta \simeq 2r\theta = 0.75 \times 10^{-3}$ cm would be large enough for the button with radius $r = 0.75$ cm. This number is very small, and practically recess is defined by the tolerances of the BPM installation. Excessive recess may, however, produce trapped modes. The decay length of the trapped mode

$$q = \zeta \frac{k_c^2 V_b}{2S}$$

depends on the parameter ζ. For a round pipe $\zeta = 1$, and for a rectangular beam pipe

$$\zeta = \frac{4a^2 \sin^2(\pi x_b/a)}{a^2 + b^2} = \frac{2a^2}{a^2 + b^2}. \tag{38}$$

The lowest TM mode in a rectangular beam pipe with dimensions $a \times b$, $a > b$ is

$$H_x = \frac{A}{b} \sin \frac{\pi x}{a} \cos \frac{\pi y}{b}, \quad H_y = -\frac{A}{a} \cos \frac{\pi x}{a} \sin \frac{\pi y}{b} \tag{37}$$

and has the cut-off frequency $(\omega_c/c)^2 = (\pi/a)^2 + (\pi/b)^2$. For four buttons with radius r located at $x = x_b = a/4$, $y = 0$ or $y = b$ and recessed by Δ, the total volume of bulging is $V_b = 4\pi r^2 \Delta$, and the decay length of the trapped mode

$$q = \zeta \frac{k_c^2 V_b}{2S}$$

is given by the parameter

$$\zeta = \frac{4a^2 \sin^2(\pi x_b/a)}{a^2 + b^2} = \frac{2a^2}{a^2 + b^2}. \tag{38}$$

The frequency shift of a mode is

$$\frac{\Delta\omega}{\omega} = \frac{(2\pi)^4 r^4 \Delta^2}{2b^4(a^2 + b^2)}. \tag{39}$$

Resistive wall gives in this case

$$(\frac{\Delta\omega}{\omega})_{RW} = \frac{\delta}{ab} \frac{a^3 + b^3}{a^2 + b^2}. \tag{40}$$

Recess is small if it gives a small frequency shift compared to the shift due to resistive wall:

$$\Delta < (\frac{b}{2\pi r})^2 \sqrt{\frac{2\delta}{ab}(a^3 + b^3)}. \tag{41}$$

Take $a = 9.0$ cm, $b = 4.8$ cm, $r = 0.75$ cm, $\delta = 1 \mu m$. Then $\Delta < 0.64 mm$ has to be taken as the maximum acceptable recess of a button in the arcs. The resistive wall frequency shift in the round pipe of the straights is

$$(\frac{\Delta\omega}{\omega})_{RW} = \frac{\delta}{2b}. \tag{42}$$

The acceptable button recess for four-button BPM in the beam pipe with radius b is

$$\Delta < \frac{b^3}{2\nu r^2}\sqrt{\frac{\delta}{b}}, \tag{43}$$

and larger than that in the arcs: $\Delta < 1.6$ mm for $b = 4.5$ cm, and $r = 0.75$ cm. The estimate of the acceptable recess is conservative and does not take into account losses to a BPM cable.

Bellows, quad/dipole offset, rf seals

We compared several designs for a bellows module. The final design uses fingers outside of the beam pipe and does not use large synchrotron radiation masks. Instead, the beam pipes are offset horizontally by a few mm and the transitions are tapered to produce sufficient protection from th synchrotron radiation (see Figs. 18 a,b).

Impedance of the quadrupole/dipole transition with the tapered beam pipe offset of 5 mm was modeled with MAFIA. The loss factor of the transition is $k_l = 4.5\,10^{-4}$ V/pC. No trapped modes were found either by considering propagation of the rf Gaussian bunch or in the S-matrix calculations.

The impedance of the bellows module is generated by finger slots, slots in the bellows corners, small tapers of the synchrotron radiation masks, and the RF seals. All contributions are small and correspond to an inductive impedance.

Impedances of the tapers of the bellow module were modeled as independent axi-symmetric structures with radii equal to the distances from the beam line to the corresponding taper. The results were then averaged proportional to the azimuthal filling factors, giving an inductance $L = 0.044$ nH and a loss factor $k_l = 3.3 \times 10^{-3}$ V/pC per bellows. For 300 bellows the total inductive impedance is only $L = 13$ nH and $k_l = 1$ V/pC. Due to the larger distance of the taper from the beam and the small vertical size of the vacuum chamber, the taper with the large 20^o angle gives only a small contribution after averaging.

Impedance of the 50 finger slots with length 1.25 cm, and width 0.76 mm is $L = 1.5 \times 10^{-4}$ nH for 50 fingers per bellows. Eight slots in the corners are wider ($w = 4$ mm) and, although they are farther away from the beam, give $L = 7.6 \times 10^{-4}$ nH per bellow, more than the finger slots. The total inductance of the slots is $L = 0.27$ nH per 300 bellows. The difference in the dimensions of the beam pipe in the arcs and straights is of no significance here.

The rf seals in a bellows module are designed to give a small 1 mm high and 0.5 mm wide recess in the beam pipe. The exact height of the recess cannot be known but the rf seal should not look like a groove that may generate trapped modes. Impedance of the rf seal is inductive[10]

$$L = \frac{4\Delta^2}{b}. \tag{44}$$

To be conservative, we take $\Delta = 1$ mm, $< 1/b >= 0.33\, cm^{-1}$. Then $L = 1.6 \times 10^{-2}$ nH per rf seal. The code ABCI gives the same $L = 1.07 \times 10^{-2}$ nH and the loss factor $k_l = 1.1 \times 10^{-4}$. Neglecting again the difference between dimensions of the bellows in the straights and arcs, we get $L = 0.47$ nH or $Z/n = 0.4 \times 10^{-3}$ Ω for the 290 rf bellows seals in the ring. (Note, that this is an overestimate of the actual impedance).

The estimate of the impedance of the rf bellows seals is valid also for the flange/gap rings. These give an additional $L = 0.47$ nH per ring. Clearly, the main issue for the bellows is not beam impedance but heating and operational reliability of the fingers.

Heating, in particular, may be produced by radiation through the slots, and by coupling of the beam to the modes of the cavity between fingers and bellow convolutions.

Radiation of the slots is dipole radiation with dipole moment induced by the field of a bunch or by the field of a TM HOM generated somewhere upstream from the bellows. The first mechanism gives the average radiated power due to the beam

$$P_{beam} = \frac{Z_0 I_{av}^2}{2\pi^{3/2}} (\frac{s_B}{\sigma_B}) (\frac{l w^2}{32 b \sigma_B^2})^2. \tag{45}$$

For $I_{av} = 3$ A, $\sigma_B = 1$ cm, and $b = 3.3$ cm that gives $P = 0.45$ W/bellows from eight corner slots. Fifty finger slots, being narrower, give less by a factor of 123.

Consider now the TM modes generated by the beam somewhere upstream at the components with a total broad-band loss factor of k_l. That defines the power of the incoming HOM modes averaged over frequencies within the bunch spectrum $P_{TM} = I_{av}^2 k_l s_B / c$. Power P_{TM} radiated from a slot due to incoming TM mode may then be compared then with power radiated by the beam P_{beam}:

$$P_{TM} = 2\sqrt{\pi} k_l \sigma_B P_{beam} \tag{46}$$

and, for the total loss factor $k_l \simeq 3$V/pC, can be larger than P_{beam} by a factor of 10.6. Radiated power becomes on the order of 5 W per bellows module. This estimate does not take into account local variation of power in TM HOM-s.

Radiation from the finger slots induced by a TE mode is 1290 times larger than radiation due to regular TM modes mostly due to the factor $(l/w)^4$. Taking into account the difference in the number of finger and corner slots, we get the power $P = 312.8$ W per bellows module, provided that the power of the incoming TE and TM modes are the same. However, beam does not couple with the TE modes: they can be produced by transformation of the TM-modes or due to decay of modes in asymmetric structures with hybrid modes. In both cases a small factor makes the power of the TE modes on the order of a few percent of the average power of the TM HOMs reducing the radiation power due to TE HOMs to a few watts per bellows module.

Another mechanism that may be important for heating is resonance excitation of eigenmodes in the cavity between fingers and bellow convolutions if their frequencies are in resonance with bunch spacing $\omega s_B/c = 2\pi n$. The enhancement factor of the power deposited by the beam is $D = 4Q_L/(2\pi n)$. For a frequency $f \simeq 1$ GHz, the factor $\omega s_B/c = 8\pi$ and D depends on the loaded Q_L, $D_{max} = Q_l/4\pi$. For a TM HOM corresponding to $k_l = 3$ V/pC, the power $P = 0.02$ W/bellows is still small even for $Q_L = 10^4$, which can be expected with stainless-steel convolutions.

Lumped pumps

Ports of the lumped vacuum pumps are screened with a grid of long and narrow slots. The layout for the straight section of the HER is shown in Fig. 19a, and for the arcs in Fig. 19b. In the arcs, there are 24 slots altogether in the upper and lower decks with length $l = 15.4$ cm and width $w = 2.54$ mm.

Impedance of each slot of the pumping screen in the arcs is $L = 1.1 \times 10^{-4}$, and the total contribution of the 24 pumping slots for all of the 200 ports in the arcs is 0.53 nH. The potential problem here is not broad-band impedance but the possibility of trapped modes.

As an example, consider a $g = 2$ cm long circular cavity with a depth $\Delta = 3$ mm in the $b = 3$ cm radius beam pipe[11]. The broad-band impedance of such a small cavity is small and mainly inductive (see Eq. (41)). However, MAFIA finds a narrow resonance with shunt impedance $R_s = 7$ $k\Omega$ and $Q = 2.7 \times 10^4$. Such a mode can be considered as a modified propagating mode with a frequency close to the cutoff frequency $\omega_m/c = \nu_0/b$ where $\nu_0 = 2.405$ is the first root of the Bessel function $J_0(\nu_0) = 0$. A small bulge of the beam pipe changes the frequency of the mode, shifting it below cutoff and making a trapped mode. The situation is analogous to the frequency shift of a mode in a cavity due to a small perturbation of the boundary. The mechanism is described in the original paper by Stupakov and Kurennoy[12]. The paper also gives a numerical example quite similar to the one described above.

The theory[12] predicts a trapped mode at the grid of the vacuum port in the arcs with shunt impedance[13] $R_s = 644.\Omega$, Q factor on the order of 3.5×10^4, and localization length $L = 35$ cm. The shunt impedance of a trapped mode at the vacuum ports of the straight sections is smaller, $R_s = 85.\Omega$. MAFIA confirms that slots cut in the circular beam pipe produce a trapped mode with parameters given by the total magnetic polarizability of the slots, Fig. 20a,b.

The frequency shift of the trapped mode is larger than the width given by the resistivity of the wall. Radiation from a narrow slot outside the thick beam-pipe is suppressed at a frequency close to the cut-off. Radiation into the beam pipe is possible only in the TE_{11} mode, which has a cut-off frequency lower than the cut-off for the TM_{01} mode. However, the width due to this process is very small. For a symmetric placement of the slots, radiation is additionally suppressed.

To eliminate trapping, the beam pipe at the vacuum port may be recessed with the recess volume equal to or slightly larger than the polarizability of the slots. Numerical simulations with MAFIA confirmed this statement[13].

A bow-like recess of the slots in the arcs has to have saggita $\Delta > 0.27$ mm and, practically, will be set to be larger than the fabrication tolerances. A mesh of small holes on the pump side should be used to prevent propagation of TE modes to the pumps.

Tapers

The circular beam pipe of the straight sections ($b = 4.5$ cm) and the rectangular beam pipe of the arcs (2.5×4.5 cm) are connected with tapers (see Fig. 21). The 2D modeling of a 10^o taper connecting two circular beam pipes with radii of 2.5 and 4.5 cm gives a conservative estimate of $k_l = 5.1 \times 10^{-3}$ V/pC and $L = 0.3$ nH per taper (see Fig. 22). The wake is inductive. The real part of the impedance is $ReZ < 0.5\,\Omega$ per taper for frequencies below 5 GHz.

Collimators

A simple model of a collimator as a pair of tapers with a height of 4.5 cm and a taper angle of 10^o gives a loss factor of $k_l = 2 \times 10^{-2}$ V/pC. The wake is inductive and corresponds to $L = 1.57$ nH per collimator (see Fig. 23).

Feedback kickers

Longitudinal and transverse kickers for PEP-II are modeled after those designed and measured for the ALS[14] (see Fig. 24). The longitudinal beam impedance of the ALS transverse kicker was found to be $Z/n = 0.53\ m\Omega$ and the loss parameter was estimated as $k_l = 0.66$ V/pC. For the longitudinal ALS kicker, $Z/n = 25\ m\Omega$ and the shunt impedance is 300 Ω within the passband 1.25 GHz.

Tolerance on the beam-pipe misalignment

Misaligned beam pipes can generate additional impedance. For a small misalignment δ of two beam pipes with radius b the impedance is inductive[15]

$$L = \frac{4}{3}\frac{\delta^2}{b}. \tag{47}$$

For $\delta = 2$ mm and $b = 2.5$ cm that gives $L = 0.023$ nH. In the worst case 300 misalignments of this kind give $L = 7$ nH, giving the upper bound for the misalignments with rms error 2 mm. We checked this formula with the 2-D code ABCI considering two pipes with radii 4.7 and 4.5 mm. That gives $L = 0.030$ nH, and the loss factor $k_l = 1.4\,10^{-3}$ V/pC. Inductance, after scaling proportional to the azimuthal filling factor 1/2 and ratio of radii is $L = 0.027$ nH in good agreement with the analytic formula.

Impedance of synchrotron radiation

Maximum value of impedance caused by synchrotron radiation

$$max(\frac{Z}{n}) = 300\frac{b}{R}\Omega \tag{48}$$

for $b = 2.5$ cm and the average radius $R = 350$ m is quite large, giving $L_{max} = 25$ nH. However, the maximum value corresponds to the harmonic number $n_{th} \simeq (\pi R/b)^{3/2} = 7.5 \times 10^6$. Such frequencies are much larger than frequencies within the bunch spectrum which, for $\sigma = 1$ cm, rolls-off starting from $n = 3.5 \times 10^4$. Impedance of the synchrotron radiation is suppressed exponentially for frequencies $n < n_{th}$ and contributes negligibly to the PEP-II impedance budget.

Cross-talk

As usual, we neglected the cross-talk between spatially close components in this calculations. An example of a periodic array of irises shows that such an interference tends to reduce the total impedance, but, to our knowledge, no serious studies of the problem are available at this time. We want to make only a few comments.

At high frequencies, a diffractional model can be used to estimate the length of the interaction of the wake with a particle. Consider, for example, a scraper with the inner radius a in a beam pipe with radius b. The angle of diffraction θ for a wave with frequency $\omega = 2\pi f$ is $\theta \simeq c/\omega a$. The elements of the vacuum system can be considered as independent if the distance between is larger than the length of diffraction $L \simeq (b-a)\omega a/c$.

If two recessed elements of the vacuum chamber are close to each other, a mode can be localized between them. However, to have a large Q factor, the mode should not be coupled with propagating modes outside of the elements. This coupling for smooth obstacles with the width w and height of the recess Δ depends exponentially on the parameter

$$\frac{\nu w}{b}\sqrt{\frac{2\Delta}{b}},$$

where b is the beam pipe radius and $\nu = 2.4$ is a root of the Bessel function. The parameter should be much larger than one for a large Q.

This problem was considered for the rf seal and recessed vacuum port. Both are short (in the model the height of each was 1 mm) and are close to each other. The field pattern found in MAFIA simulations confirmed, as was expected, that such a system does not confine a mode (see Fig. 26).

Summary

The main contributions to impedance of PEP-II come from the rf cavities and the resistive wall impedance. Components giving the main contribution to inductive part of the impedance are summarized in Table 6. The contribution of an element is calculated and multiplied by the number of such elements given in Table 2. These elements are mainly inductive but do have a small resistive part, which give a non-zero loss factor of $k_l = 3.1$ V/pC. We can describe this loss by a constant resistivity R_Ω.

Longitudinal impedance is the sum of the narrow-band and the broad-band impedances. The narrow-band impedance is given by the modes of the cavities (see Table. 3), and a few modes in the BPMs, and kickers. Broad-band longitudinal impedance can be parametrized[16] [17] by expansion over $\sqrt{\omega}$. For $\omega > 0$ it takes the form:

$$Z_l(\omega) = -iZ_0\frac{L\omega}{4\pi c} + (1-i)R_W\sqrt{\omega} + R_\Omega + (1+i)R_c\sqrt{\frac{\omega_c}{\omega}}\theta(\omega - \omega_c) + \ldots.$$

where $Z_0 = 4\pi/c = 120\pi\ \Omega$, and $\omega_c/2\pi$ is a cutoff frequency. Usually, the impedance can be set to the cutoff frequency of the beam pipe at the rf cavities. Dependence of the total impedance on the choice of ω_c is weak if the number of modes below cutoff taken into account in the narrow-band impedance and the coefficient R_c are chosen consistently.

The first term in the expansion of Z_l over $\sqrt{\omega}$ describes inductive impedance generated by all elements in the ring with eigenfrequencies much higher than frequencies within the bunch spectrum. The inductance L (L in nH, 1 cm=1 nH) defines the low-frequency parameter Z_l/n where $n = \omega/\omega_0$ is the harmonic number, and $\omega_0 = 2\pi f = c/R$ is the revolution frequency.

The inductance L is given by Table 6. The second term describes the resistive wall impedance. The third term describes a constant resistivity. The wake of a bunch in this case is proportional to $\rho(s)$. The last term is a good parametrization of the high-frequency tail of the rf cavities.

Transverse impedance is dominated by the modes of the rf cavities, Table 4, and resistive wall estimated above. The rest of the ring contributes little and, therefore, it may suffice to have an estimate of such a contribution. This estimate can be obtained in a standard way from the results of Table 6.

Table 6. The main contribution to the inductive impedance of PEP-II

		L (nH)	k_l (V/pC)
	Dipole screens	0.10	
	BPM	11.	0.8
	Arc bellow module	13.5	1.41
	Collimators	18.9	0.24
	Pump slots	0.8	
	Flange/gap rings	0.47	0.03
	Tapers oct/round	3.6	0.06
	IR chamber	5.0	0.12
	Feedback kickers	29.8	0.66
	Injection port	0.17	0.004
	Abort dump port	0.23	0.005
Total		83.3	3.4

REFERENCES

1. PEP-II, An Asymmetric B Factory, CDR, LBL PUB-5379, SLAC-418, June 1993.
2. R. L. Gluckstern, J. van Zeijts, B. Zotter. Coupling Impedance of Beam Pipes of General Cross Section, CERN SL/AP 92-25, June 1992.
3. J. Byrd, G. Lambertson. Resistive wall impedance of the B Factory, PEP-II AP Note 9-93, March 1993.
4. J.D. Jackson, SSC Central Design Group Report, SSC-N-110 (1986), E. D. Courant, M. Month, BNL-50875, 1978.
5. E. Henestroza, S. Heifets, M. Zolotarev Trapped Modes in the PEP-II B Factory Interaction Region, PAC, Washington, 1995.
6. A. Kulikov, J. Seeman, M. Zolotarev. PEP-II Abort System Specifications, PEP-II Note 61, 10/1994.
7. A. Piwinsky, IEEE Nucl. Sci., 24, No. 3, 1364, 1977.
8. S. Kurennoy, Beam-Coupling Impedance of Holes in Vacuum-Chamber Walls, IHEP 92-84, UNK, 1992.
9. N. Kurita, D. Martin, C.-K Ng, S. Smith, and T. Weiland. Simulation of PEP-II Beam Position Monitor, PEP-II Note 87, March 1995.
10. K. Bane. The Calculated Longitudinal Impedance of the SLC Damping Ring, SLAC-PUB-4618, 1988.
11. Cho K. Ng and T. Weiland. Impedance analysis of the PEP-II Vacuum Chamber, SLAC report, unpublished, 1994.
12. G. V. Stupakov, S. S. Kurennoy. Trapped EM Modes in a Waveguide with a Small Discontinuity, SSCL-Preprint-459, June 1993.
13. S. Heifets, G. Stupakov. Study of the Trapped Modes at the Vacuum Ports, PEP-II Note No. 80, January 1995.
14. J. Corlett, J. Johnson, G. Lambertson, F. Voelker. Longitudinal and Transverse Feedback Kickers for the ALS, LBL-34955, UC-410, 1994.

15. J.F. Crawford. The electro-Magnetic Properties of Vacuum Chambers, TM-12-90-04, Paul Scherrer Institute, November 1991.

16. S. Heifets Broad band Impedance of the B Factory, SLAC/AP-93, February 1992.

17. S. Bartalucci, M. Serio, B. Sparato, M. Zobov, L. Palumbo. Broad-band model impedance for DAPHNE Main Rings, Nucl Inst. and Methods, A337, 1994.

18. R. L. Gluckstern. Preprint CERN SL/92-05 (AP), Geneva, 1992.

19. M. Sands. Preprint PEP-253, SLAC 1977.

20. K. Bane, P.B. Wilson, and T. Weiland. Wakefields and Wakefield Acceleration, SLAC-PUB-3528, 1984.

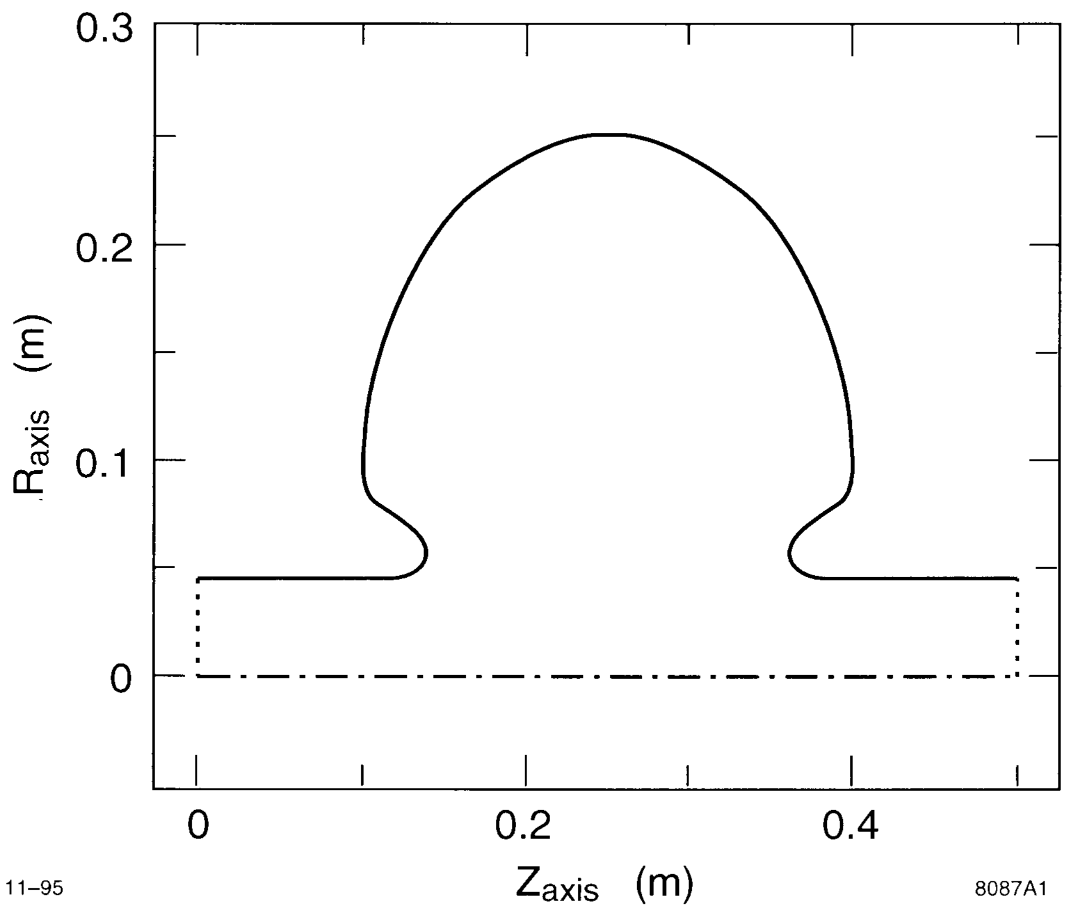

Figure 1. RF cavity shape (without damping ports).

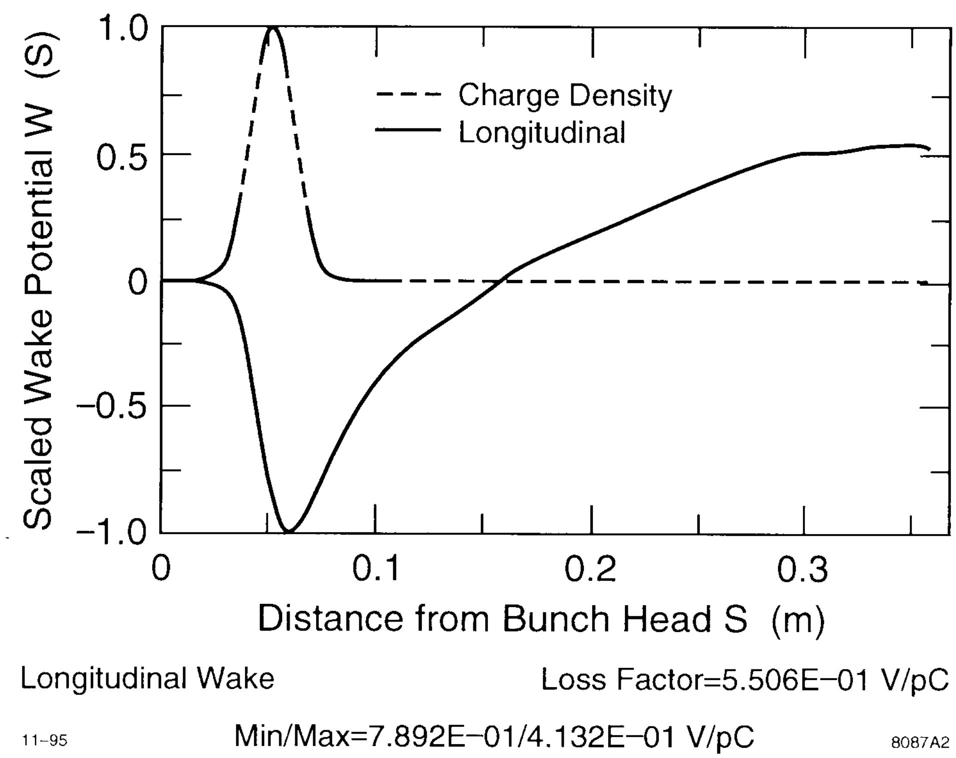

Figure 2. Broad-band longitudinal wake potential of a rf cavity.

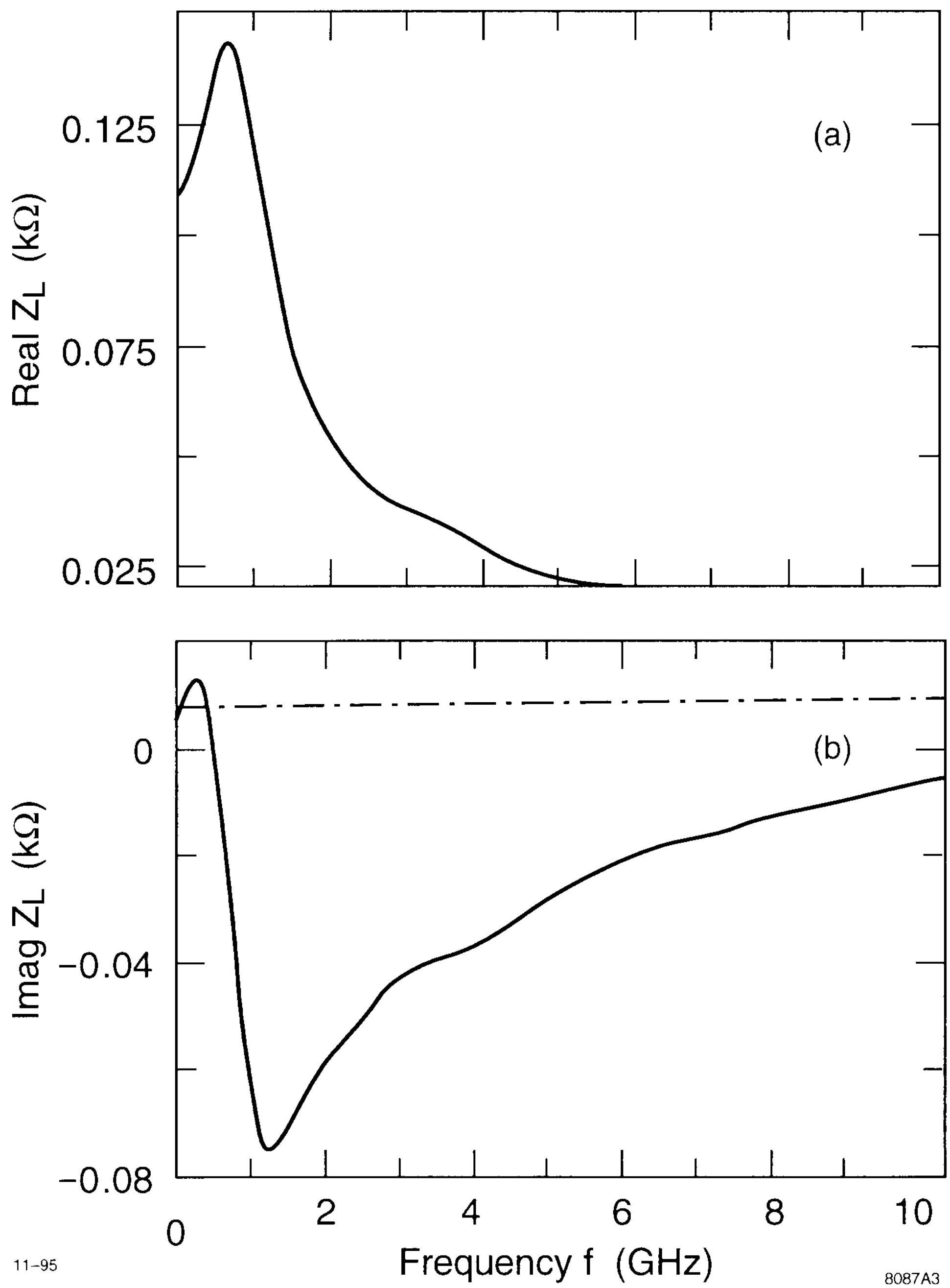

Figure 3. Dipole wake potential of a rf cavity.

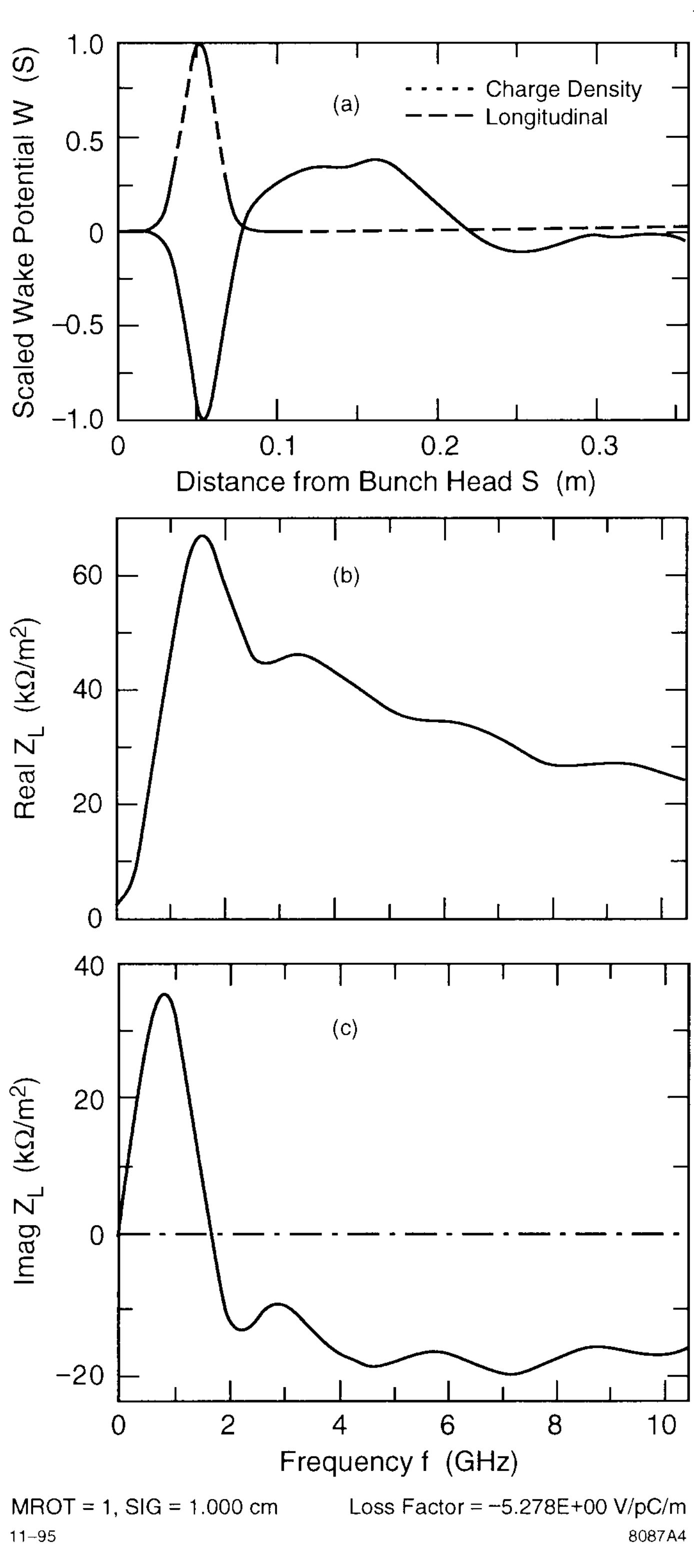

Figure 4. Real part of the longitudinal broadband impedance of a rf cavity.

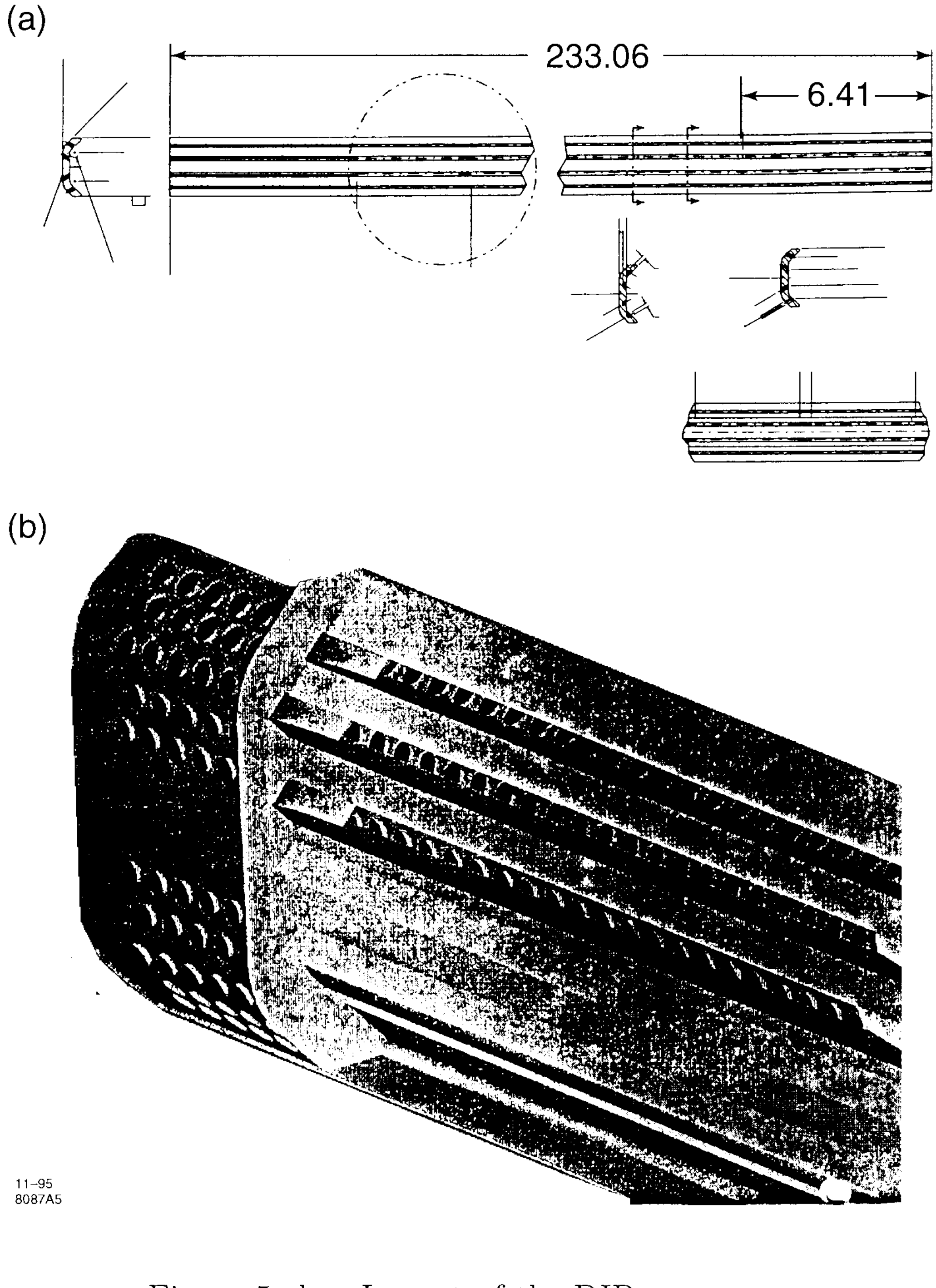

Figure 5a,b. Layout of the DIP screen.

(a)

(b)

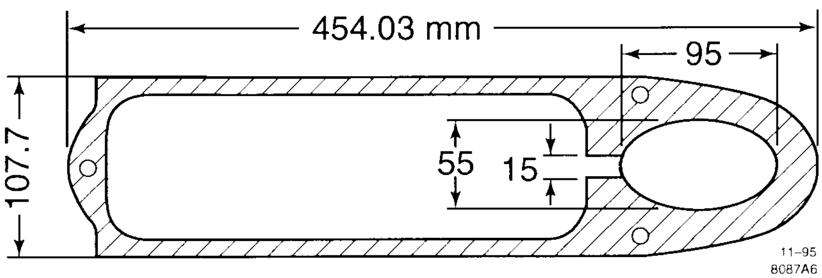

Figure 6a,b. Layout of the LER antechamber.

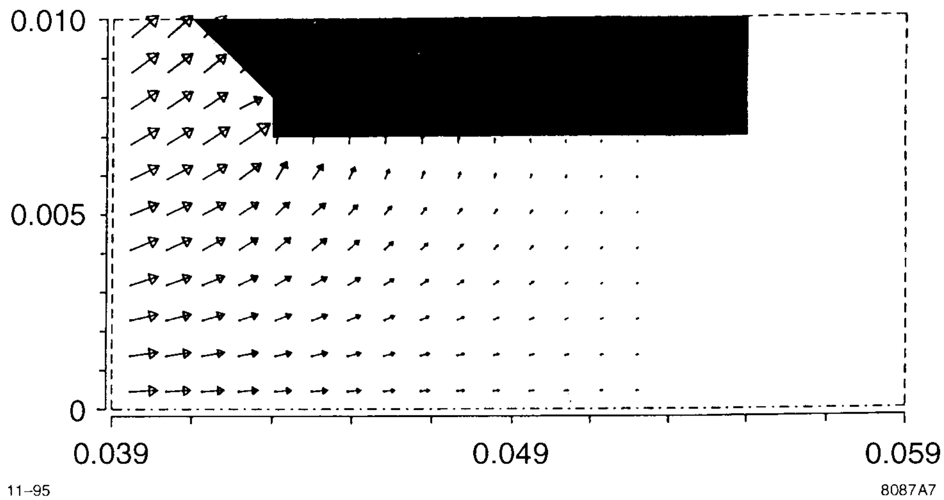

Figure 7. Electric field pattern for the antechamber.

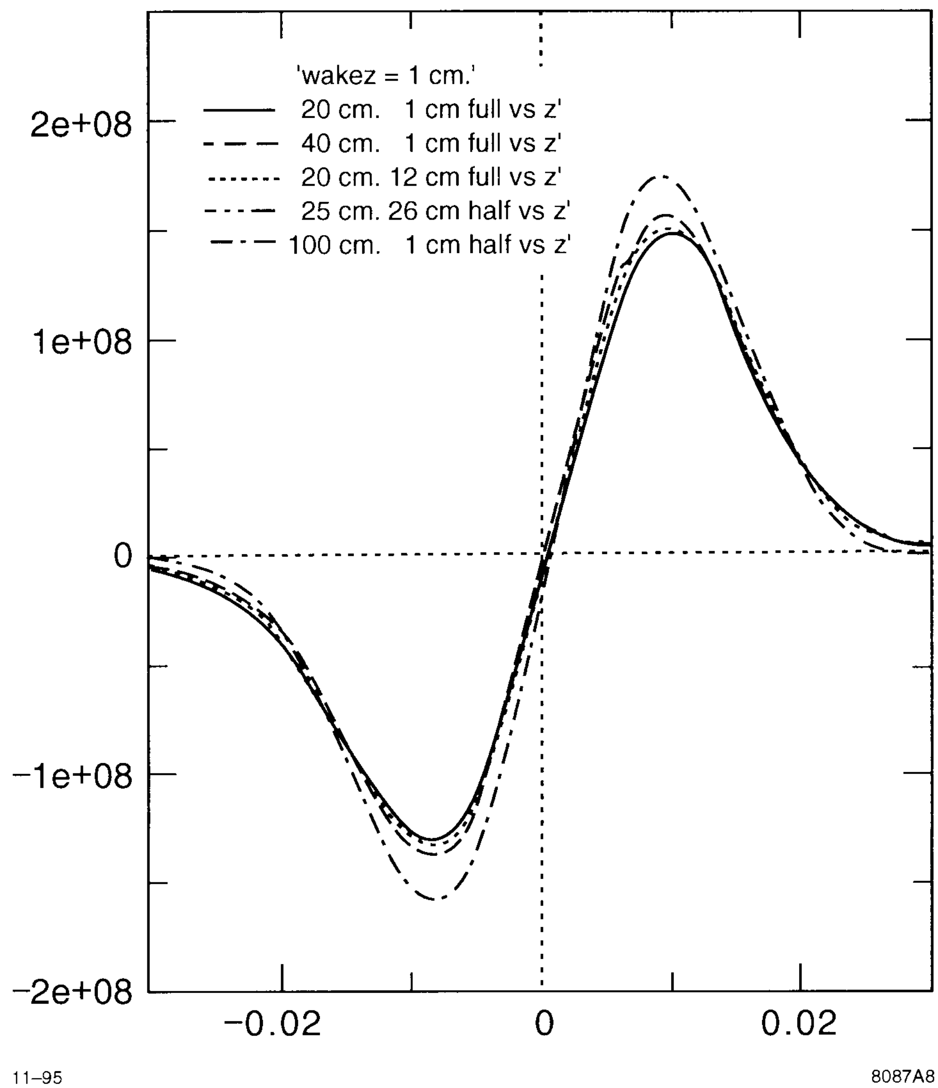

Figure 8. Longitudinal wake potential $W(s)$ for different lengths and depths of the antechamber.

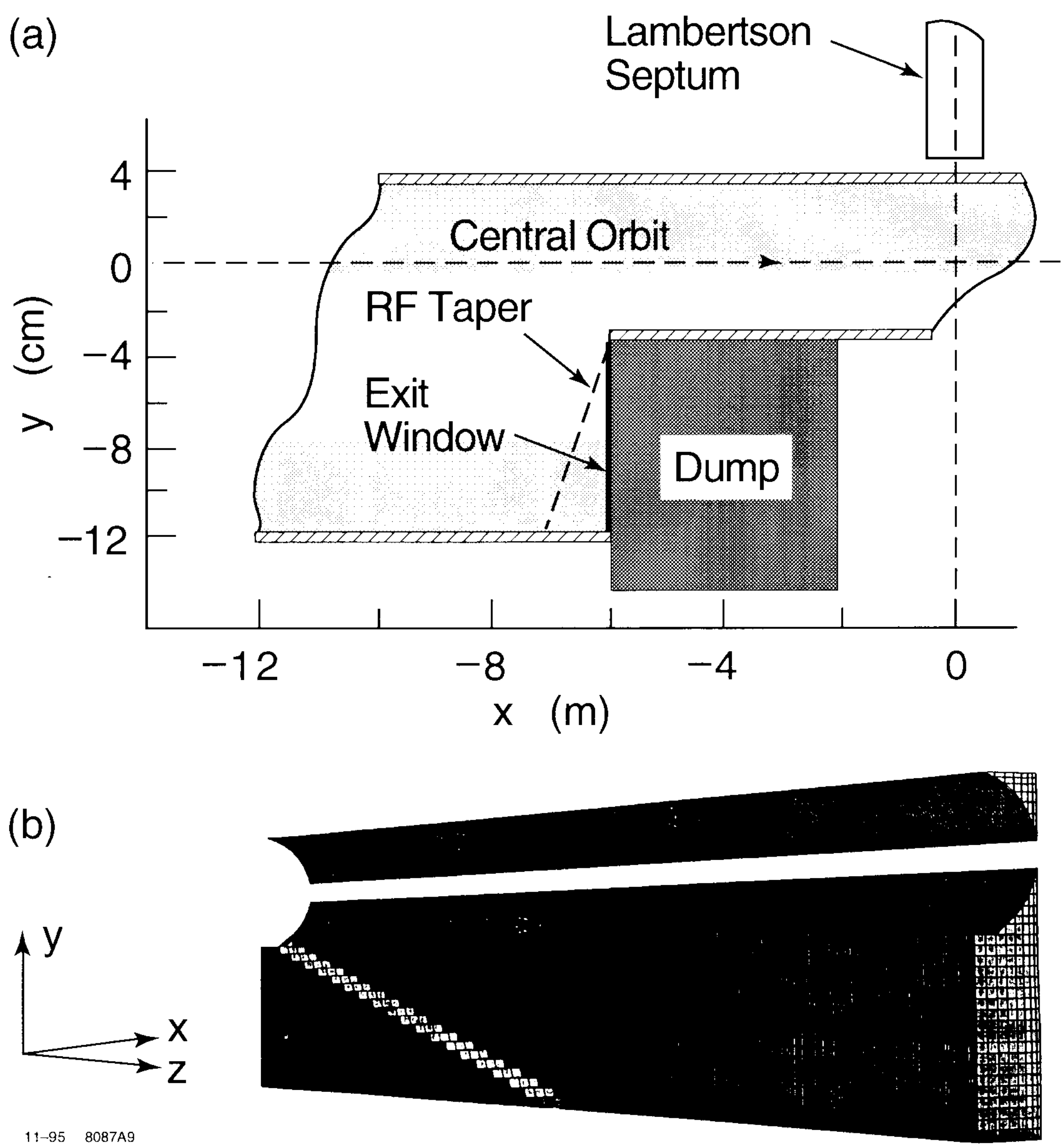

Figure 9a,b. Layout of the abort system and the model used in MAFIA simulations.

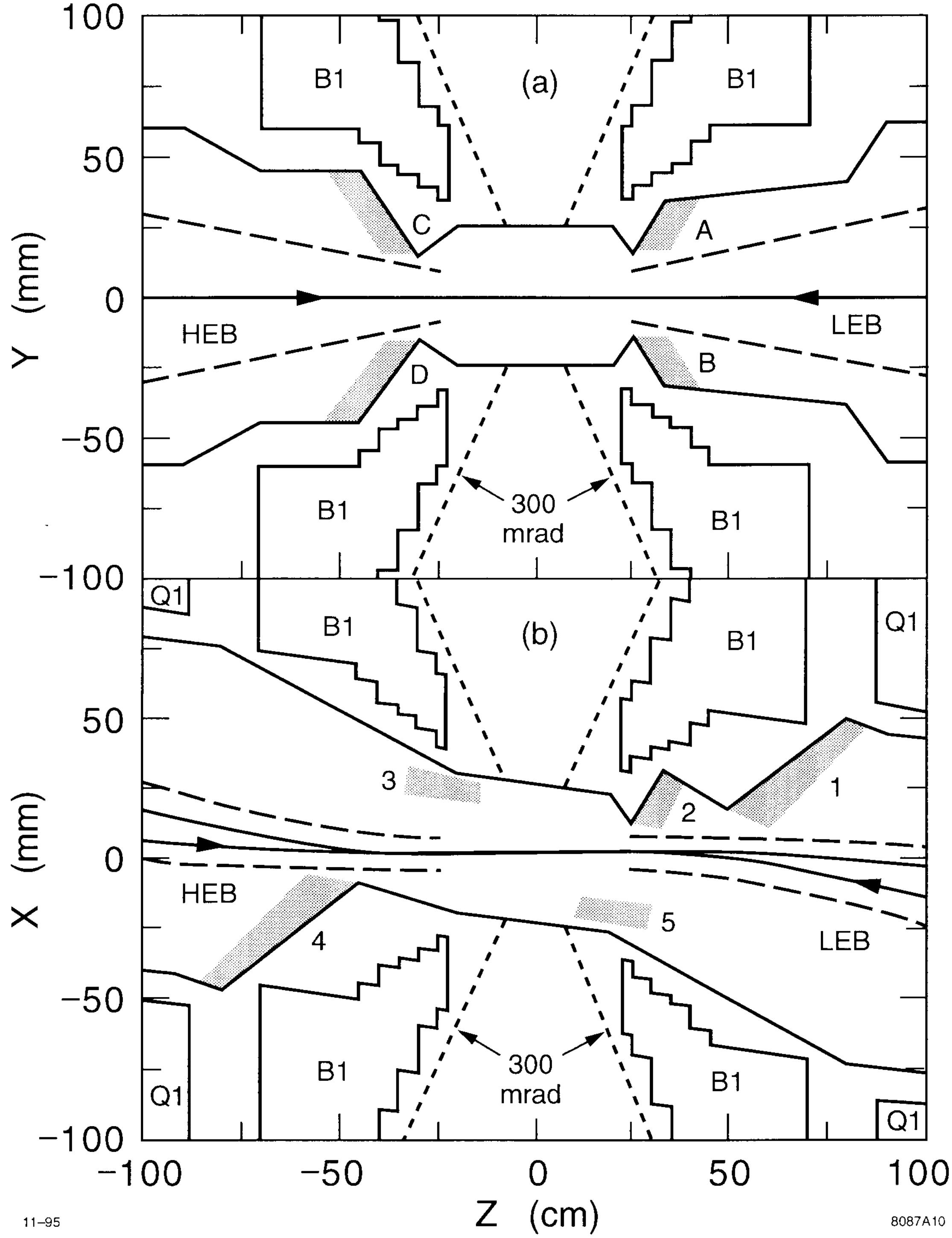

Figure 10a,b. Layout of masks of the IR in horizontal and vertical planes.

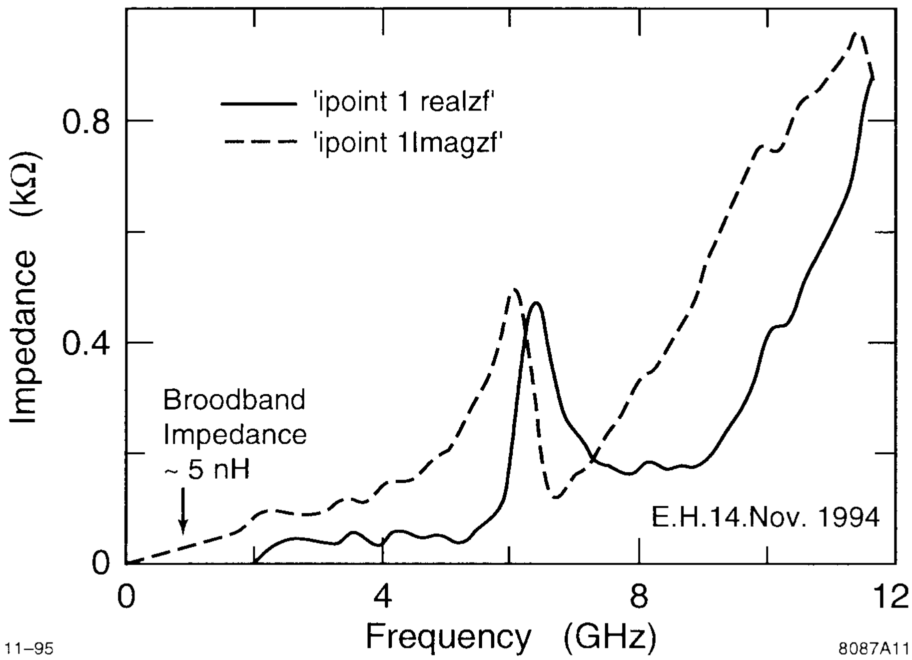

Figure 11. Broadband impedance of the IR.

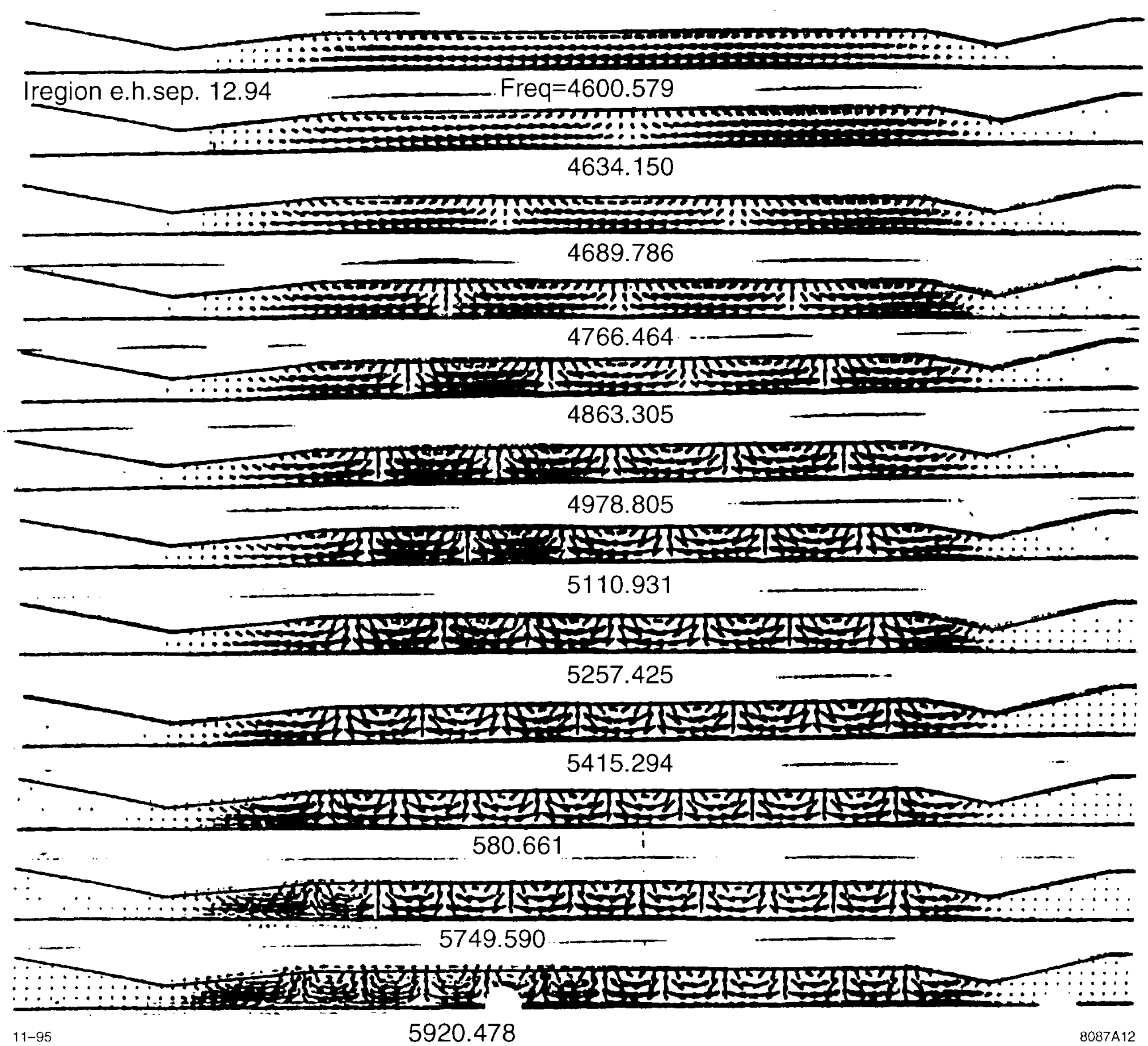

Figure 12. Field pattern of trapped modes of the Be pipe of the IR.

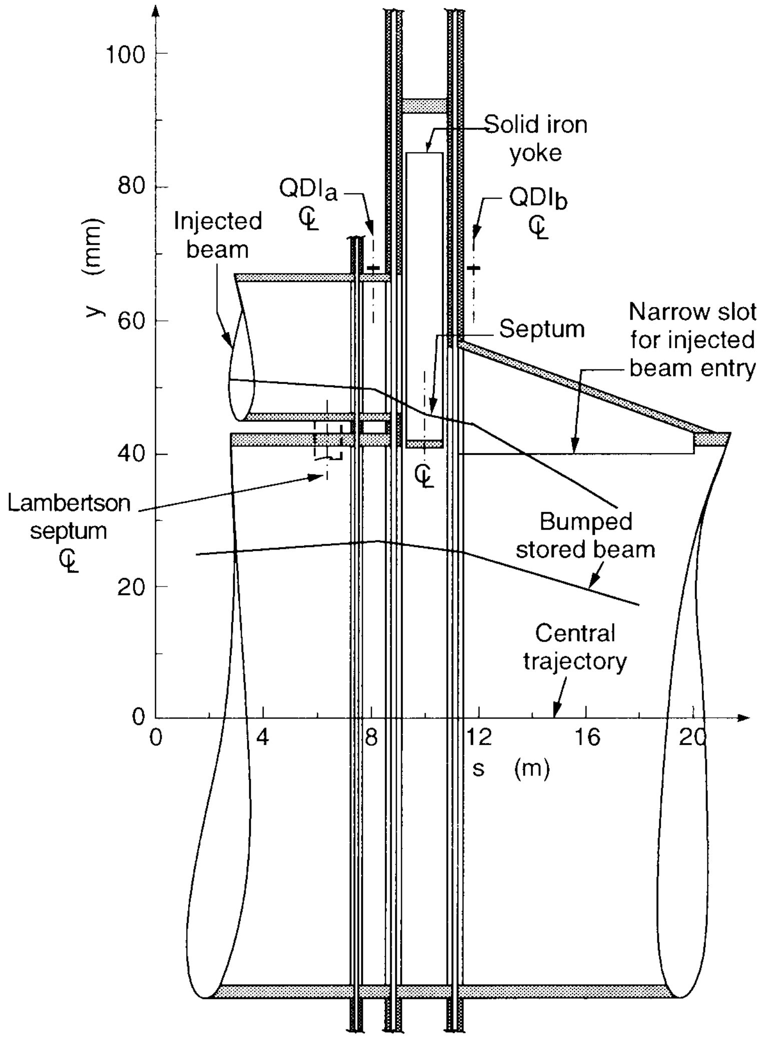

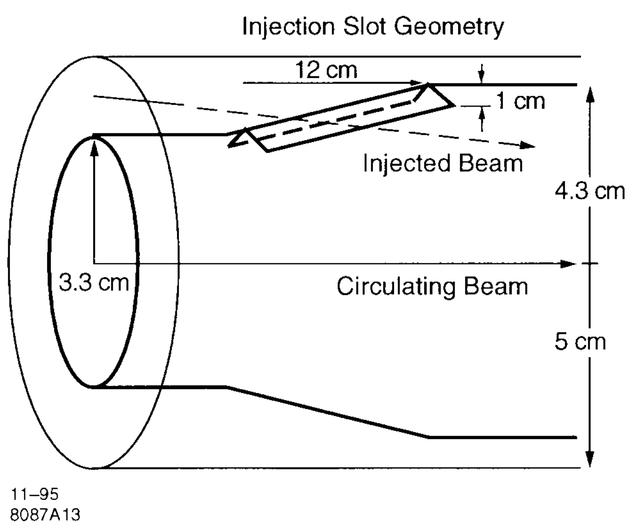

Figure 13a,b. Injection port and the model used in MAFIA simulations.

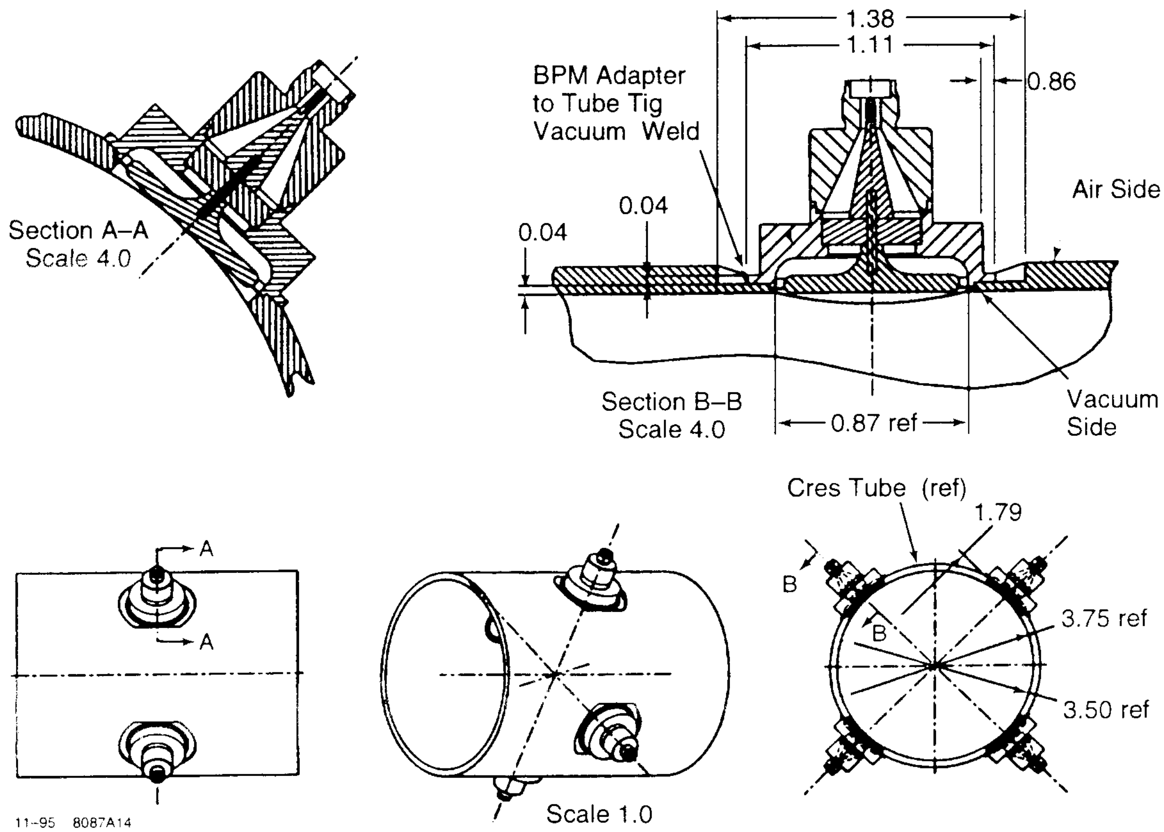

Figure 14. Layout of a four button BPM.

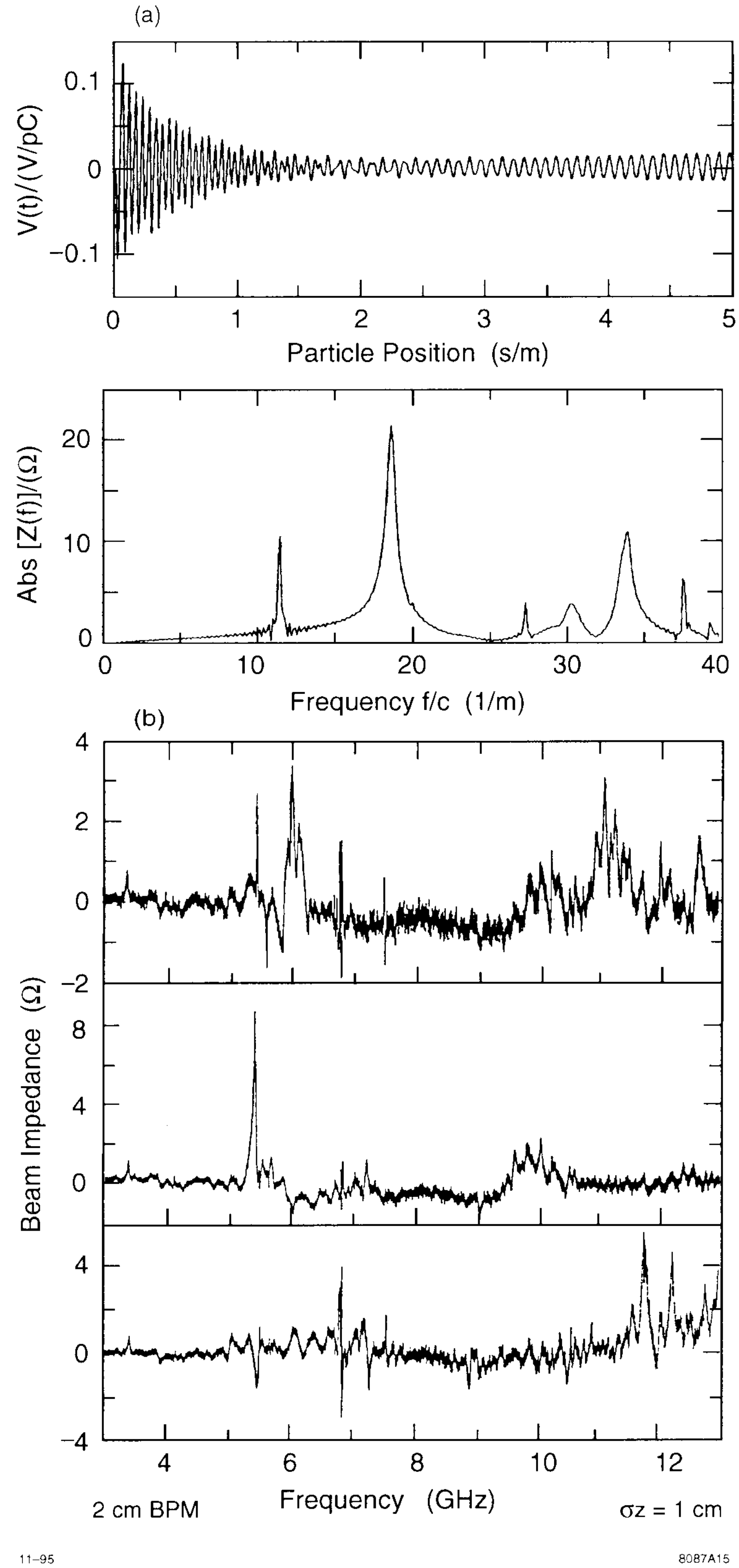

Figure 15a,b. Comparison of MAFIA simulations with the wire measurements of a BPM.

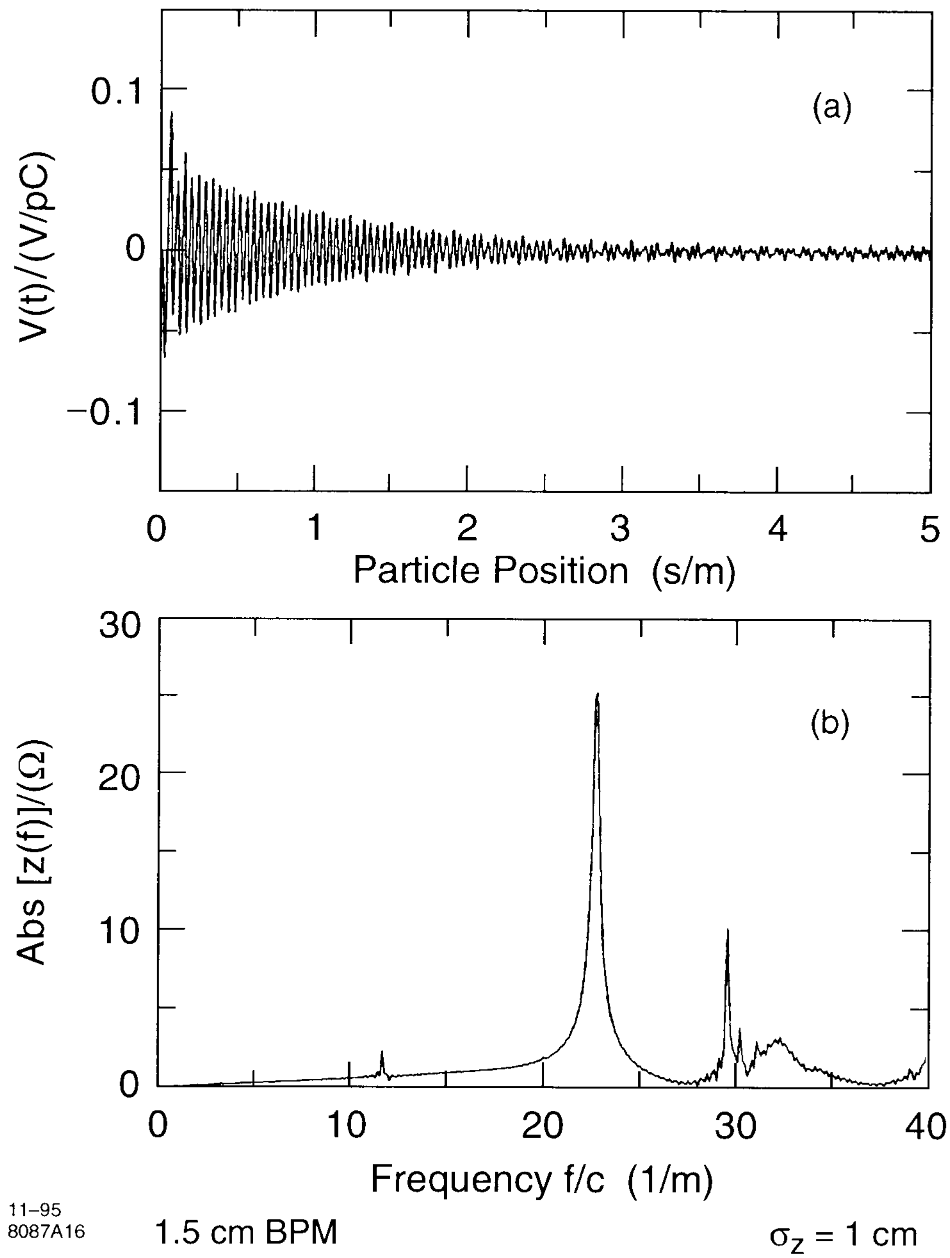

Figure 16. Impedances and wakefields of a 1.5 cm button.

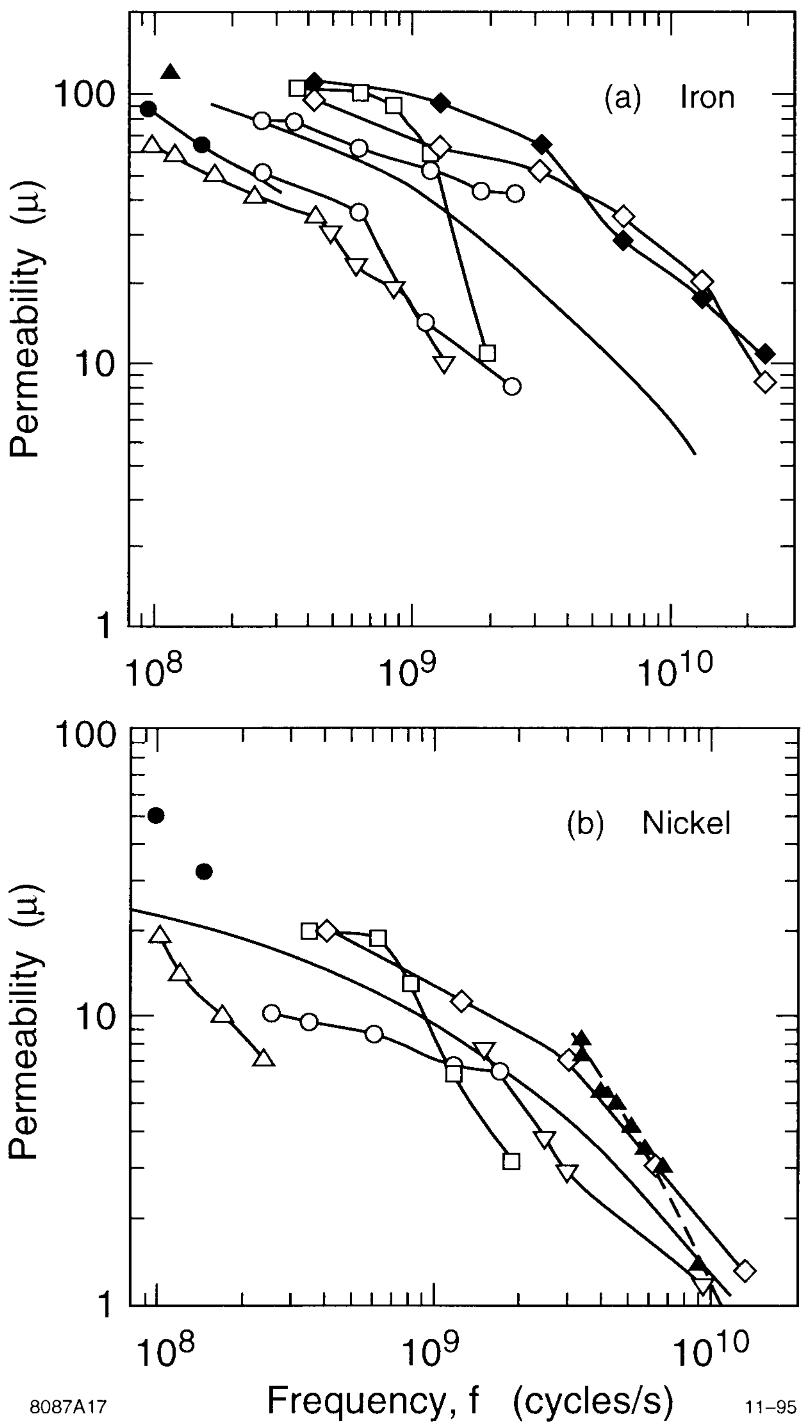

Figure 17. Dependence on frequency of the permeability μ.

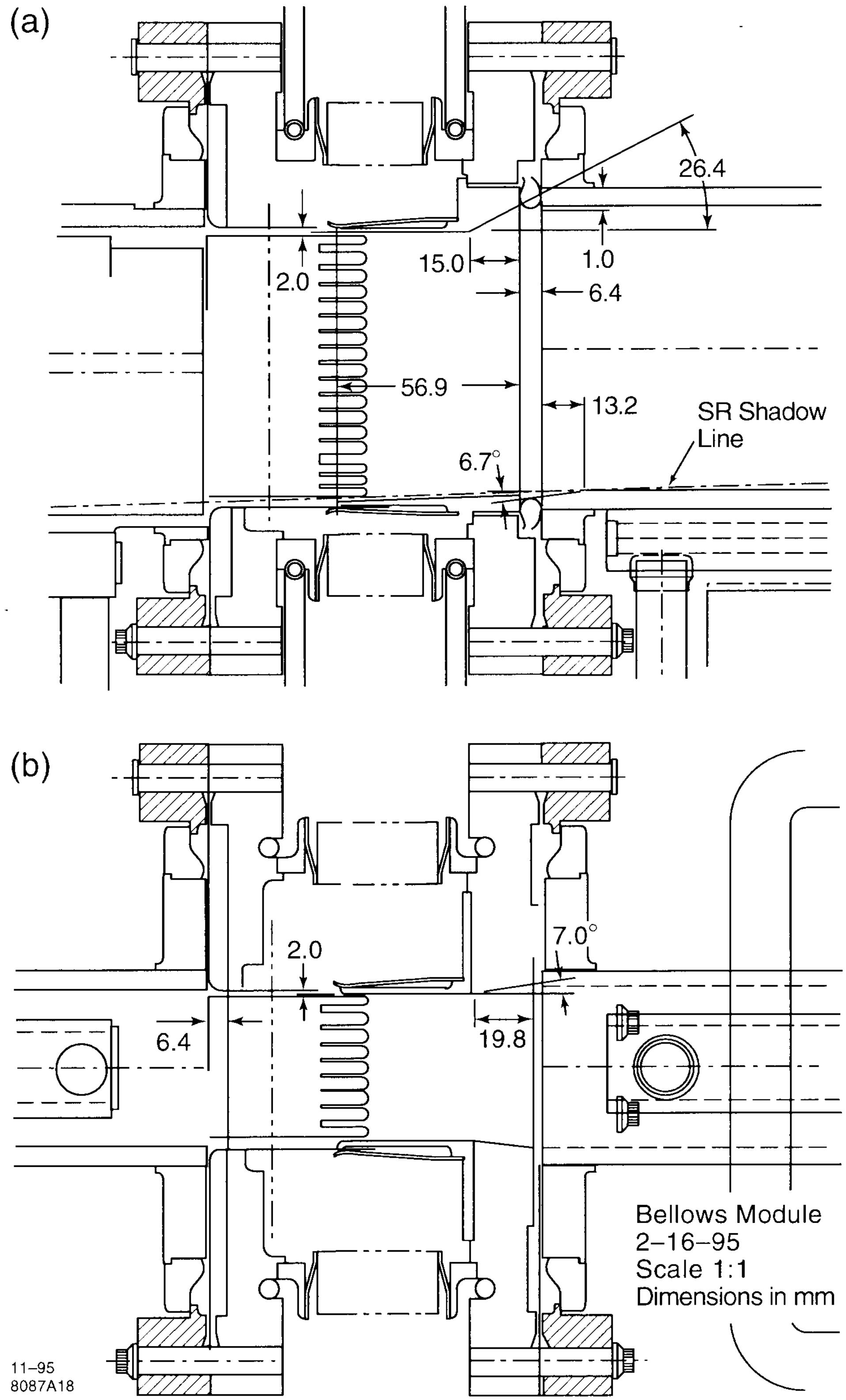

Figure 18a,b. Layout of a bellows, x, z and y, z planes.

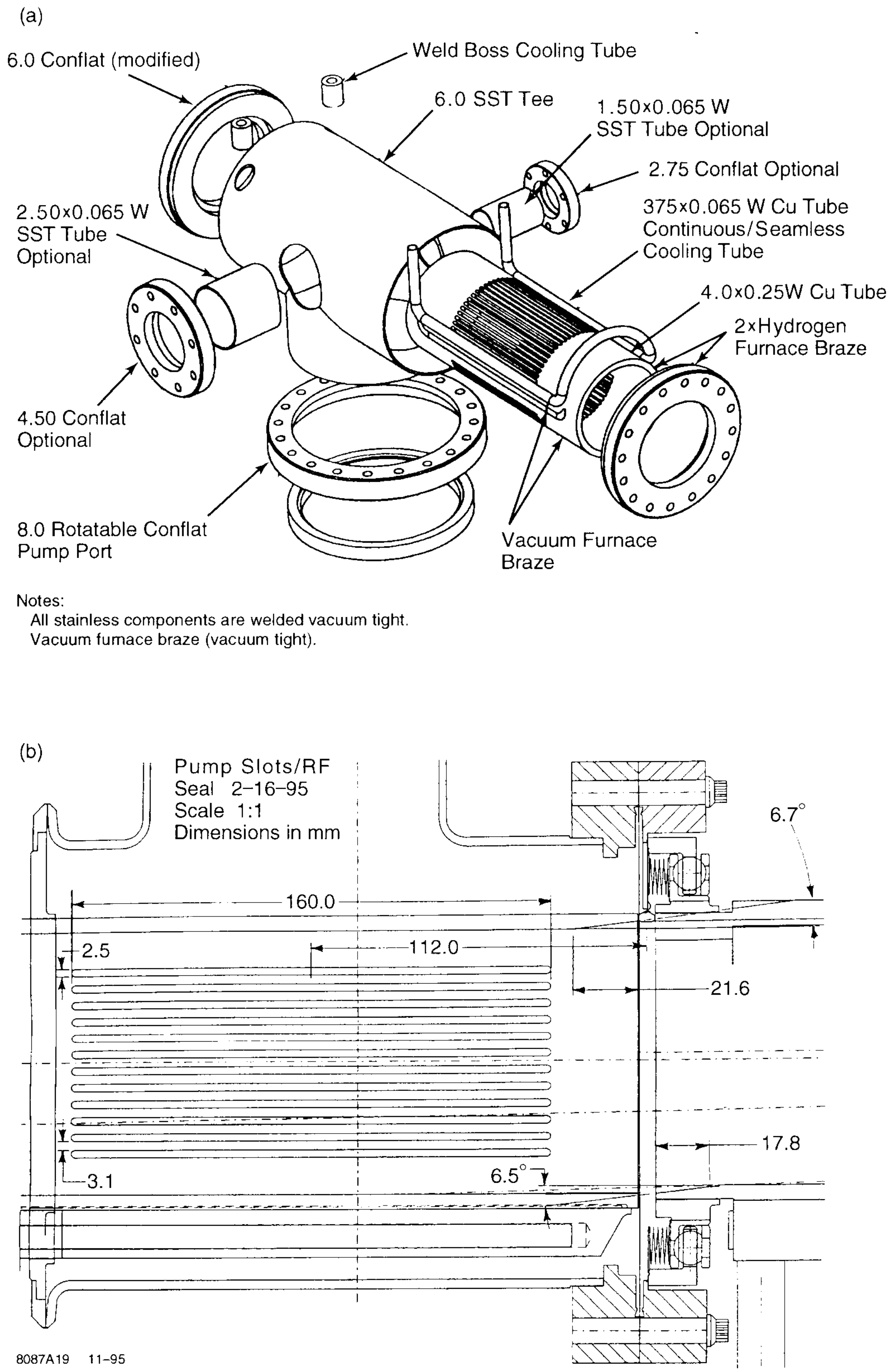

Figure 19a,b. Layout of the slots of a vacuum port for the straight sections

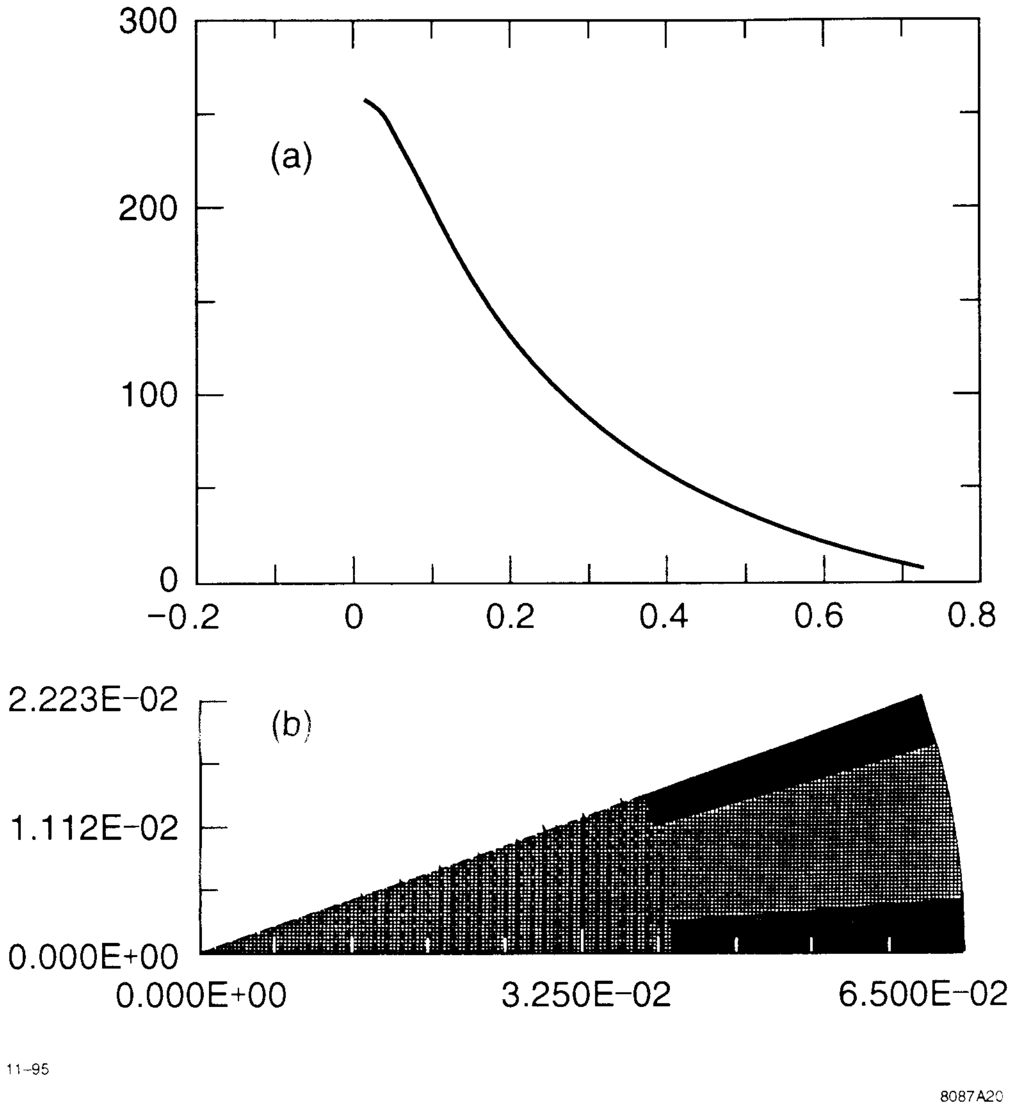

Figure 20. (a) Dependence of the E_z component of a trapped mode on the distance from the slot center and (b) the electric field pattern.

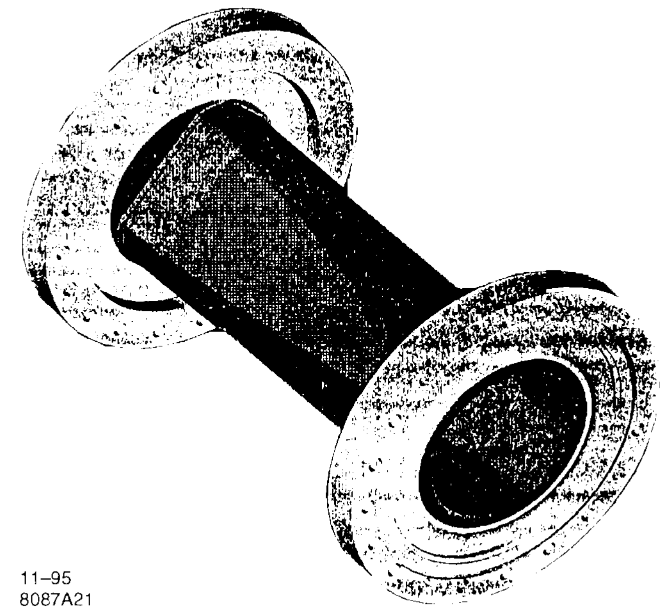

Figure 21. Layout of the taper of a transition from a round to a hexagonal pipe.

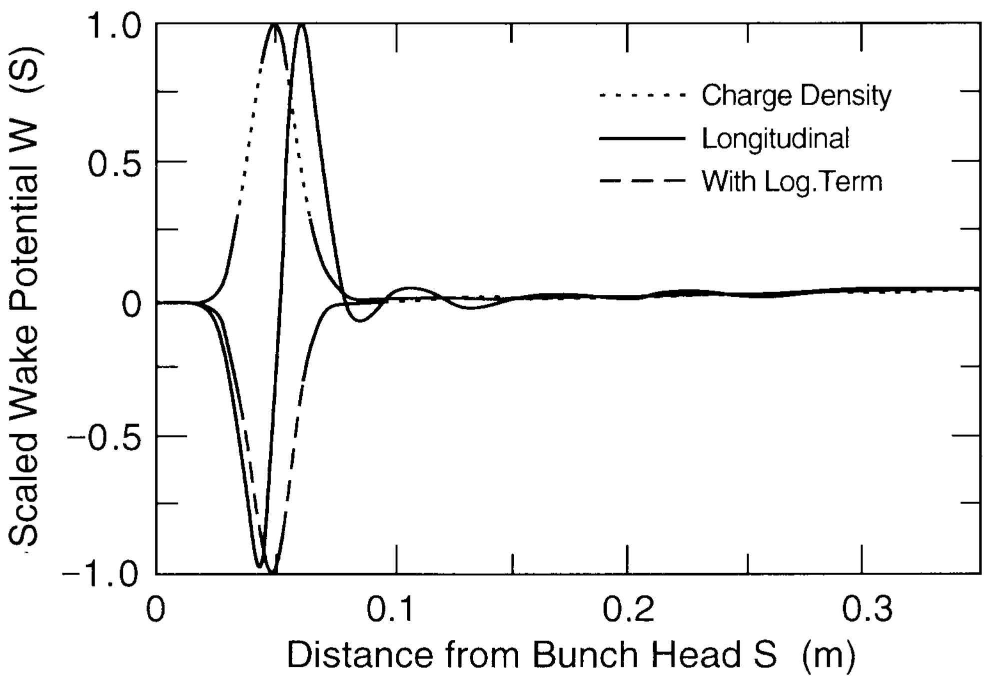

	Min/max	Loss Factor
Longitudinal Wake	–7.056E–02/7.634E–02 V/pC	–5.097E–03 V/pC
With log term	–4.546E–01/3.287E–03 V/pC	–3.031E–01 V/pC

11–95

8087A22

Figure 22. Wake potential of the taper.

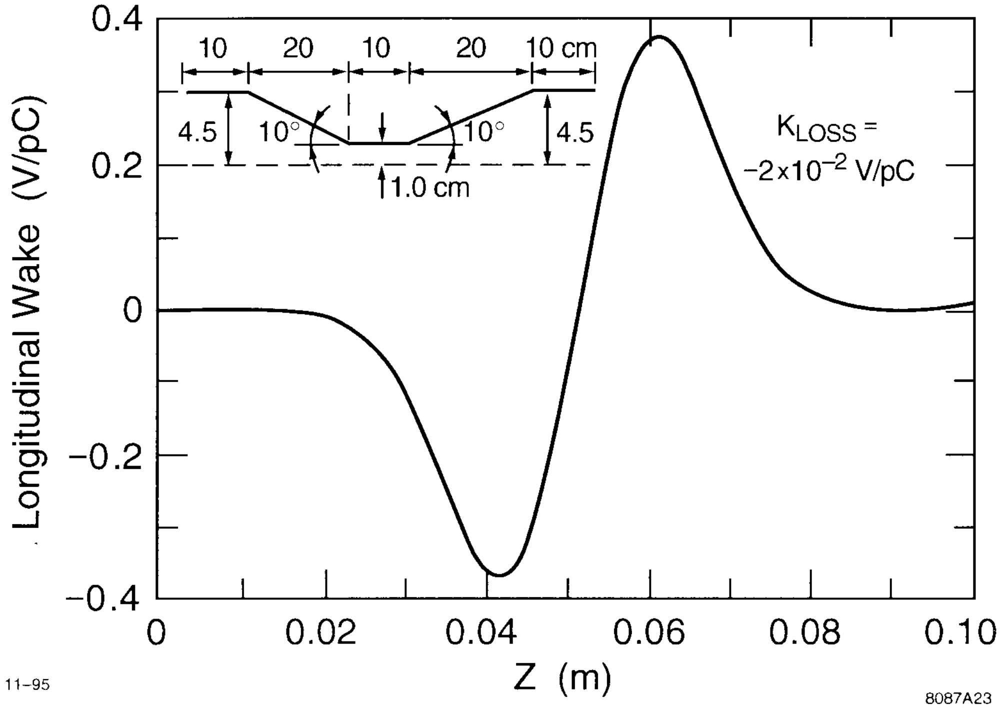

Figure 23. Longitudinal wake potential of a model of a typical collimator.

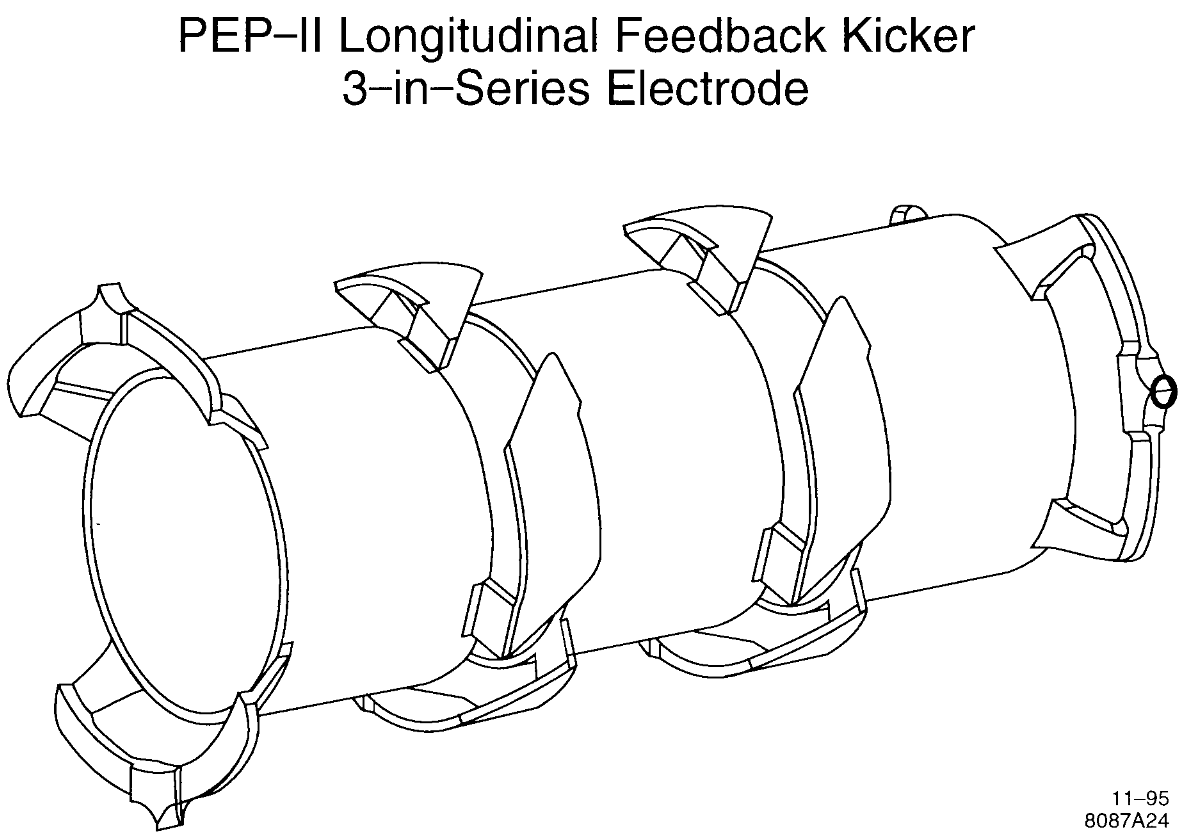

Figure 24. Layout of a feedback kicker.

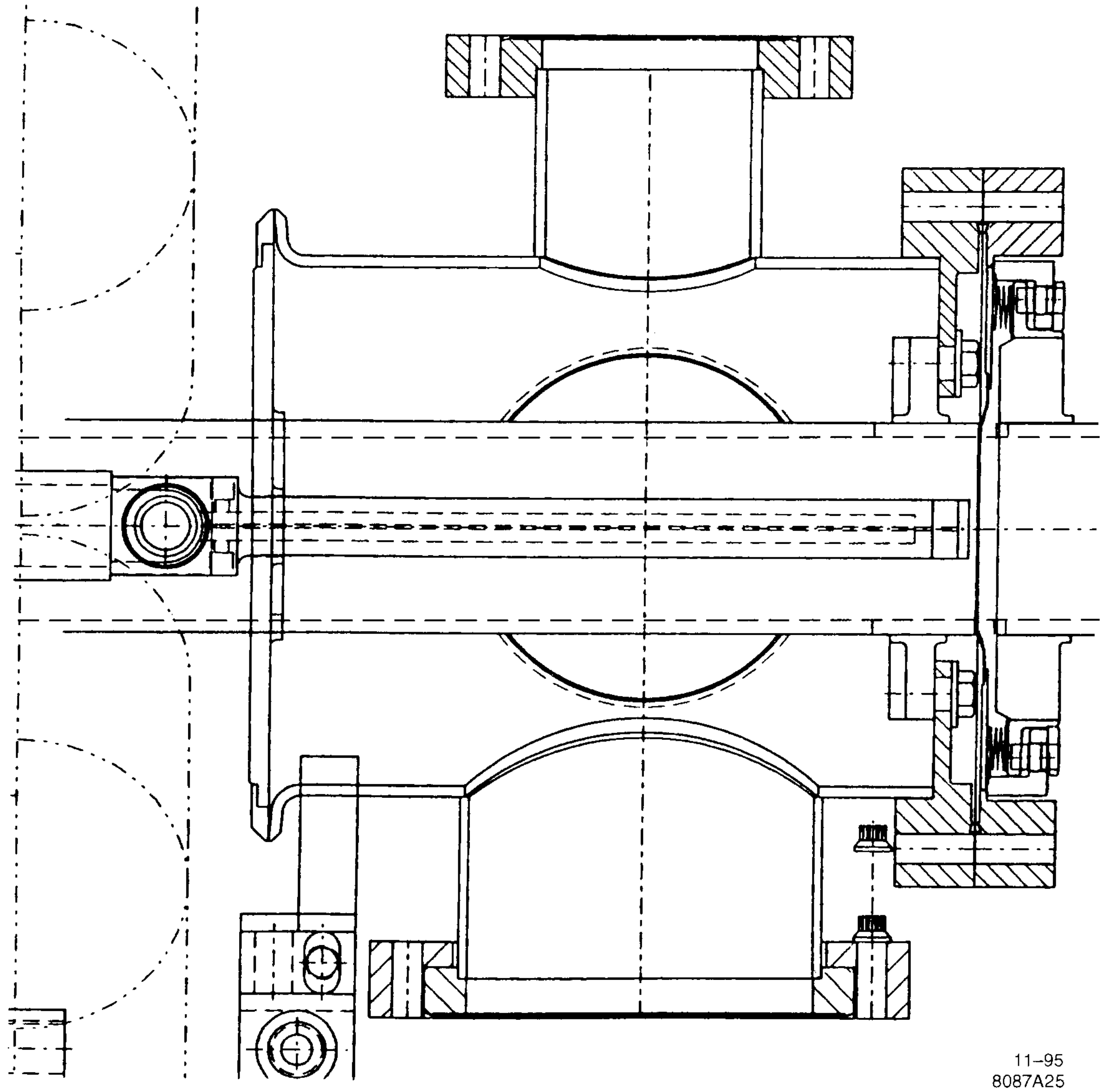

Figure 25. Layout of a valve.